Relation between Snow and Winter Soil-Surface Temperatures in Tundra Landscapes: Results of Observations in Northern Alaska

By Kristen Alice Pyne

B.A. in Geography, May 2012, University of South Florida

A Thesis submitted to

The Faculty of
The Columbian College of Arts and Sciences
of the George Washington University
in partial satisfaction of the requirements
for the degree of Master of Arts

May 18, 2014

Thesis directed by

Nikolay Shiklomanov
Professor of Geography

© Copyright 2014 by Kristen Alice Pyne
All rights reserved

Acknowledgements

This research was funded through the U.S. National Science Foundation (NSF) Office of Polar Programs under grants OPP-0095088 and OPP-0352958 to the University of Delaware, ARC-1002119 and ARC-1204110 to The George Washington University. I am grateful to the CH2MHILL Polar Services and UMIAQ for providing logistics and to BP Alaska for granting access to the Prudhoe Bay Oil Field.

I would like to thank my advisor Professor Nikolay Shiklomanov of the George Washington University, Department of Geography for encouraging me and helping me complete this thesis. I would also like to thank Professor Anna E. Klene of the University of Montana Department of Geography, and Dmitry Streletskiy of the George Washington University.

Abstract of Thesis

"Relation between Snow and Winter Soil-Surface Temperatures in Tundra Landscapes: Results of Observations in Northern Alaska"

Continuous spatial monitoring of air and soil-surface temperatures under natural covers (vegetation and snow) was conducted at an array of Arctic Alaskan sites representing a range of undisturbed tundra landscapes since 1995. This data set was utilized to assess the complex relation between snow cover and the winter ground-surface temperature regime. Snow cover has a strong influence on soil-surface temperatures during the winter by slowing the heat transfer between the atmosphere and ground. A range of direct observational methods and analytical techniques was used to assess snow thickness and duration. The annual duration of snow cover at each site was determined by calculating change in soil-surface temperature amplitudes. A vertical array of Thermochron IButton® temperature loggers, arranged from the soil-surface to 1 meter above the surface and time-lapse digital cameras were installed at observational sites in 2010-2012 to assess snow depth. Supplementary snow-depth information derived from direct observations and winter precipitations obtained from nearby USDA SNOTEL sites was used to estimate snow depth during the study period. The snow and soil-surface temperature records were used to calculate several indexes (e.g., n-factors, temperature/degree days offsets, etc.) suitable for quantitative assessment of the temporal and spatial variability in the interaction between snow and soil-surface temperatures in characteristic tundra landscapes of the North Slope of Alaska.

Key Words: Cryosphere, Arctic Alaska, Snow, Temperature

Table of Contents

Acknowledgements iii

Abstract of Thesis iv

List of Figures viii

List of Tables xi

List of Equations xii

I. Introduction 1

II. Hypothesis and Objectives 3

III. Study Area 5

III.1 The Kuparuk River Region 5

III.2 Study Sites 7

IV. Air and Soil-Surface Temperature Observations 11

IV.1 Introduction 11

IV.2 Background 12

IV.2.1 General Temperature Trends on the Alaskan North Slope 12

IV.2.2 Spatial Variability of Air Temperatures in the Kuparuk Region 13

IV.2.3 Variability of Soil-Temperatures in the Kuparuk Region 13

IV.3 Methodology 15

IV.3.1 Data Availability 15

IV.3.2 Data Analysis 18

IV.4 Results 19

IV.4.1 Spatial Variability of Observed Air Temperatures 19

IV.4.2 Temporal Variability of Observed Air Temperatures 22

IV.4.3 Spatial Variability of Observed Soil-surface Temperatures 26
IV.4.4 Temporal Variability of Observed Soil-surface Temperatures 29
IV.5 Conclusions 35
V. Snow-Cover Characteristics 36
V.1 Introduction 36
V.2 Background 37
V.2.1 Changes in Snow-Cover Characteristics 37
V.2.2 Importance of Snow 39
V.2.3 Snow Accumulation 40
V.2.4 Current Techniques used to Monitor Snow-Cover Characteristics 41
V.3 Methodology 44
V.3.1 Data Availability 44
V.3.2. Data Analysis 47
V.4 Results 53
V.4.1 Snow-Cover Duration from Air and Soil-Surface Temperatures 53
V.4.2 SCD and Snow Depth from Vertical Arrays of Temperature Dataloggers. 61
V.4.3 SCD and Snow Depth from Time-lapse Cameras and SNOTEL Data 66
V.5 Conclusion 77
VI. Relations Between Soil-Surface Temperatures and Snow-Cover Characteristics. 79
VI.1 Introduction 79
VI.2 Background 79
VI.3 Methodology 81
VI.3.1 Data Availability 81

VI.3.2 Data Analysis 81
VI.4 Results 83
VI.5 Conclusions 93
VII. Conclusions 94
VII.1 Summary of Results 94
VII.2 Suggestions for Future Research 95
VIII. References 96

List of Figures

Figure III-1 Location of Kuparuk river region on the North Slope of Alaska. 7

Figure III-2 Location of the CALM study sites in the Kuparuk region utilized in this study. Bioclimatic subzones and physiographic boundaries are shown. 10

Figure IV-1 Location of CALM study sites used to observe air and soil-surface 17

Figure IV-2 Mean annual (a), summer (b), and winter (c) air temperatures observed at study sites between 1996 and 2013. 20

Figure IV-3 Mean annual (a), summer (b), and winter (c) air temperatures in subzone D between 1996 and 2013. 23

Figure IV-4 Mean annual (a), summer (b), and winter (c) air temperatures observed in subzone E between 1996 and 2013. 25

Figure IV-5 Mean annual (a), summer (b), and winter (c) soil-surface temperatures 27

Figure IV-6 Mean annual (a), summer (b), and winter (c) soil-surface temperatures 31

Figure IV-7 Annual (a), summer (b), and winter (c) soil-surface temperatures observed in subzone E between 1996 and 2013. 34

Figure V-1 Map showing the locations of SNOTEL sites and CALM study sites instrumented with iButtons and cameras, in the Kuparuk region. Bioclimatic subzones and the physiographic boundary are shown. 46

Figure V-2 Three stakes situated at different micro-topographic heights in front of the time-lapse camera at U32a (a), U32b (b), U11b (c), U11c (d), U10 (e) and U31 (f) ……..50

Figure V-3 The maximum, mean, and minimum SCD in subzone E between 53

Figure V-4 Maximum, mean, and minimum dates of snow onset estimated in subzone D between 1996 and 2013. Years when two or fewer study sites were able to have snow onset determined are represented as single points 54

Figure V-5 Maximum, mean, and minimum dates of snowmelt estimated in subzone D between 1996 and 2013. Years when two or fewer CALM study sites were able to have the date of snowmelt determined are represented as single points on the graph and were not utilized to calculate the trend. 55

Figure V-6 Maximum, mean, and minimum SCD estimated in subzone E between.... 57

Figure V-7 Maximum, mean, and minimum dates of snow onset estimated in subzone E between 1996 and 2013. 58

Figure V-8 Maximum, mean, and minimum dates of snowmelt estimated in subzone E between 1996 and 2013. 59

Figure V-9 Annual number of freeze/thaw cycles estimated in subzones D and E between 1996 and 2013. 60

Figure V-10 Snow-pack development at site U11b in subzone E. Snow depths were interpolated from mean daily temperatures recorded by the vertical 63

Figure V-11 Temperature records from the vertical iButton array showing data utilized to estimate (a) snow onset and (b) snowmelt at site U11b in subzone E. 65

Figure V-12 Snow depth at sites U31 (a), U32b (b) and U11b (c), observed using time-lapse cameras during the 2013 hydrologic year. SNOTEL precipitation and snow depth data collected at Prudhoe Bay (a), Sagwon (b), and Imnavait (c) are also shown.. 69

Figure V-13 Accumulated precipitaiton observed at SNOTEL sites in Prudhoe Bay, Sagwon, and Imnavait between 1996 and 2013. 70

Figure V-14 Relation of SNOTEL snow depth and accumulated precipitation data from the 2012 and 2013 hydrologic years at Prudhoe Bay, Sagwon, and Imnavait. 71

Figure V-15 Mean maximum, mean, and minimum snow-depth progression at Prudhoe Bay (a), Sagwon (b), and Imnavait (c) calculated using SNOTEL accumulated precipitation and the regression equations from each SNOTEL site. 73

Figure V-16 Maximum snow depth estimated and observed at SNOTEL sites between 2005 and 2013.. 74

Figure V-17 Change in estimated snow depth versus precipitation at Prudhoe Bay (a), Sagwon (b), and Imnavait (c), using SNOTEL data. 76

Figure VI-1 Box-and-whisker plot showing the median, quartiles, and range of FDD_a at each of the 9 CALM sites observed between 1996 and 2013. Sites are shown in a north-south transect (left to right). 83

Figure VI-2 Box-and-whisker plot showing the median, quartiles, and range of FDD_s at each CALM site observed between 1996 and 2013. Sites are shown in a north to south progression (left to right). 84

Figure VI-3 A time-series of winter n-factors at sites between 1996 and 2013 86

Figure VI-4 Time-series of mean winter n-factors for subzones D and E between.... 88

Figure VI-5 Correlation between mean annual winter n-factors and estimated 89

Figure VI-6 Box and whisker plot showing the median, quartiles, and range of winter n-factors at each CALM site observed between 1996 and 2013. Sites are listed in a north to south progression (left to right). 90

Figure VI-7 Relation between FDD_a and winter n-factors between 1996 and 2013 at CALM sites……91

Figure VI-8 Relation between FDD_s and winter n-factors at CALM sites between 1996 and 2013……92

List of Tables

Table III-1 Characteristics of the nine CALM sites used in this study. 9

Table IV-1 Mean annual, summer, and winter air temperatures observed at study sites between 1996 and 2013. 21

Table IV-2 Mean annual, summer and winter soil-surface temperatures observed at study sites between 1996 and 2013. 29

Table V-1 Table showing CALM sites where iButtons were installed (N.A. means no iButtons installed). The number of iButtons in the array from which data were successfully retrieved at each site is shown. 61

Table VI-1 Winter n-factor minimum, mean, median, maximum, range and standard deviation observed between 1996 and 2013 at each site, which are listed 85

Table VI-2 Summary statistics of winter n-factors observed in subzones D and E between 1996 and 2013. 87

List of Equations

Equation VI-1..... 81

I. Introduction

Results from the recent Intergovernmental Panel on Climate Change (IPCC) report indicate that global mean surface temperatures have increased 0.72 °C over the time period 1951 to 2012 (Hartmann et al., 2013). The effects of these warming temperatures are expected to be intensified in the Arctic, making the region extremely important for climate studies (Olsen et al., 2011; Sazonova and Romanovsky, 2003). Generally, the Arctic climate is characterized as having low precipitation totals that range from 100 to 150 mm annually (Maxwell., 1992). Mean annual air temperatures are also low, with extremely cold winters well below -20 °C and cool summers (McBean, 2005). The climate in this region is greatly influenced by the high reflectivity of snow on the ground, which lasts for approximately 8 to 10 months during the year (Callaghan et al., 2011a).

One of the features in the Arctic that is being significantly altered by global warming and is a major concern to scientists is permafrost, and its changing properties are very difficult to monitor. Permafrost is any material within the ground that remains permanently frozen for at least two years. Above the permafrost there is a layer of ground that thaws during the summer and refreezes during the winter and is known as the active layer (Shiklomanov and Nelson, 2013).

The major effects on permafrost as a result of increasing global temperatures have been well documented (Olsen et al., 2011; Romanovsky et al., 2010; Shiklomanov et al., 2010; Zhang et al., 2013). Permafrost temperatures across Northern Hemisphere high latitude regions have increased in recent decades (Romanovsky et al., 2010, Shiklomanov

et al., 2010). Increases in permafrost temperatures of about 1.5 to 2.5 °C were observed in Northern Alaska between 1985 and 2000, and this warming continued into the 2000s at a more moderate rate (Smith et al., 2010). The increasing permafrost temperatures are consistent with the increasing measurements of active-layer thickness in the Arctic (Olsen et al., 2011, Zhang et al., 2013). The warming permafrost temperatures and increasing active-layer thicknesses are forcing the southern boundary of continuous permafrost to slowly make its way further north. As permafrost temperatures warm and the active layer thickens, areas of continuous permafrost are transitioning into zones of discontinues and absent permafrost (Throop et al., 2011).

Warming soil temperatures along with the melting of excess ice commonly found in the upper portion of the permafrost in high latitudes will promote widespread ecological disturbance (Shiklomanov and Nelson, 2013). This will lead to changes on plant rooting systems, soil nutrient availability, and the carbon and water cycles (Decker et al., 2003; Sazonova and Romanovsky, 2003). Warming soils will also increase the extent of thermokarst terrain in the Arctic. Thermokarst occurs when the underlying ground ice melts, causing the land to change topography as the ground subsides, and past studies have indicated ground subsidence as a result of this melting (Shiklomanov and Nelson, 2013; Streletskiy et al., 2008). As the active layer thickens, the melting of deeper frozen soil layers also releases stored carbon (in the form of methane or carbon dioxide) into the atmosphere, creating a positive feedback to global warming (Gouttevin et al., 2012).

Unlike much of the cryosphere, which lies above the soil-surface and is influenced directly by climate, permafrost receives a climatic signal that is modified by

vegetation and snow. Past studies have addressed the effect of vegetation on the ground thermal regime in Northern Alaska (Klene et al., 2001; Nyland et al., 2012; Streletskiy et al., 2008). The effect of snow on the ground thermal regime has been documented (Morse et al., 2012) however, studies on the effect of snow on the ground temperatures in Northern Alaska are limited because of the little availability of snow cover data. This thesis addresses snow, its depth and duration, and the effect it has on soil-surface temperatures within the study area.

II. Hypothesis and Objectives

Extensive research has been done characterizing the major climatic, surface, and subsurface conditions in the Kuparuk River watershed of the Alaskan North Slope. Previous studies on subsurface conditions have shown variation in active-layer thickness within the region (Streletskiy et al., 2008). Currently, there is limited information on snow cover in the Kuparuk, and snow-cover measurements have only recently begun being taken at some point locations. Being that snow warms the underlying ground in the winter, soil-surface temperatures are expected to be warmer in areas with thick snow covers. The central topic addressed in the present study *is the spatial and temporal variability of soil-surface temperatures at a regional scale, and the effect of snow cover upon this variability.* The research has the following objectives:

1. Analyze empirical data to capture spatial and temporal variability of air and soil-surface temperatures within the study area.

2. Use ground-based observations to describe snow-cover duration and snow depth in the region.
3. Using available snow depth and precipitation data, extrapolate long-term snow-depth estimates at representative study sites.
4. Relate long-term snow depth measurements to long-term soil-surface temperature variability.

This research is based primarily upon long-term observations conducted at a series of Circumpolar Active Layer Monitoring (CALM) sites in the Kuparuk Region on the Alaskan North Slope. A detailed description of the CALM study sites used in this analysis is provided in Chapter III. Each objective is addressed in a chapter that describes the corresponding background, methodology, and results. Chapter IV analyzes the variability of long-term air and soil-surface temperatures between 1995 and 2013. Chapter V describes snow cover measurements made using several different observational methodologies at the study sites, and available snow depth and precipitation data from national observational networks. Long-term soil-surface temperatures are related to snow-depth measurements in Chapter VI.

III. Study Area

III.1 The Kuparuk River Region

The study area for this project is located in the Kuparuk region on the North Slope of Alaska, between the Brooks Mountain Range and the Arctic Ocean. The Kuparuk River watershed is 26,278-km^2 and contains the entire drainage system for the Kuparuk River. Modern industrial development in the region began with the first successful oil well in Prudhoe Bay in 1968 and subsequent construction of the Trans-Alaska Pipeline and accompanying Dalton Highway, which made the area more accessible and promoted research in the region. The North Slope experiences a cold arctic climate, and winter air temperatures in the Kuparuk Basin decrease 3 °C from south to north, and snow depths also decrease. Coastal areas also experience a 15 day longer winter season than inland areas near the Brooks Range (Sturm et al., 2005).

In 1995, nine 1-hectare flux plots were established in the Kuparuk River basin to represent the range of land-cover types in the area. The North Slope of Alaska has three physiographic provinces, including the poorly drained Arctic coastal plain, the Arctic foothills, and the northern portion of the Brooks Range. The Kuparuk region transects all three, but a lack of data and the rough topography in the Brooks Range prevents this physiographic region from being included in the study.

The Arctic coastal plain is poorly drained with many thaw lakes, and it is very wet and marshy in the summer. Maximum altitude on the plain reaches < 200 m in the south, and non-acidic soils dominate. This region has an arctic climate with very low mean annual air temperature and annual precipitation. Winds are also continuous and strong.

The Arctic foothills have a better-defined drainage pattern than the coastal Plain and fewer lakes. The Arctic foothills are further divided into two sections based on elevation. The southern foothills range from 180 m to 365 m, while the northern foothills range from 1,200 to 3,500 feet (Wahrhaftig, 1965). The Arctic foothills show a sharp contrast in substrate chemistry and are generally non-acidic (pH > 6.5) in the north and acidic (pH < 5.5) in the south (Walker et al., 1998).

The North Slope is divided into tundra bioclimatic subzones C, D and E, which are distinguished based upon differences in dominant vegetation and mean summer temperature. Subzone C located along the arctic coastline is 5 to 50 % covered with vascular plants, and contains prostate and hemi-prostrate dwarf shrubs up to 15 cm. Subzone D is 50 to 80 % covered with vascular plants with a dwarf shrub layer 10 to 40 cm. While subzone E is 80 to 100 % covered with vascular plants consisting of low-shrubs up to 80 cm (Walker et al., 2005). Figure III-1 displays the location of bioclimatic subzones on the North Slope, the physiographic boundary dividing the Arctic coastal plain from the foothills, and the Kuparuk River region. Being that the Kuparuk River Basin is underlain by permafrost and is distributed across diverse settings with differences in topography and vegetation, it is well suited for this study. The area also had existing databases with air and soil-surface temperature records dating back to 1995.

Figure III-1 Location of Kuparuk river region on the North Slope of Alaska. Bioclimatic subzones and the physiographic boundary dividing the Arctic coastal plain and the foothills are shown.

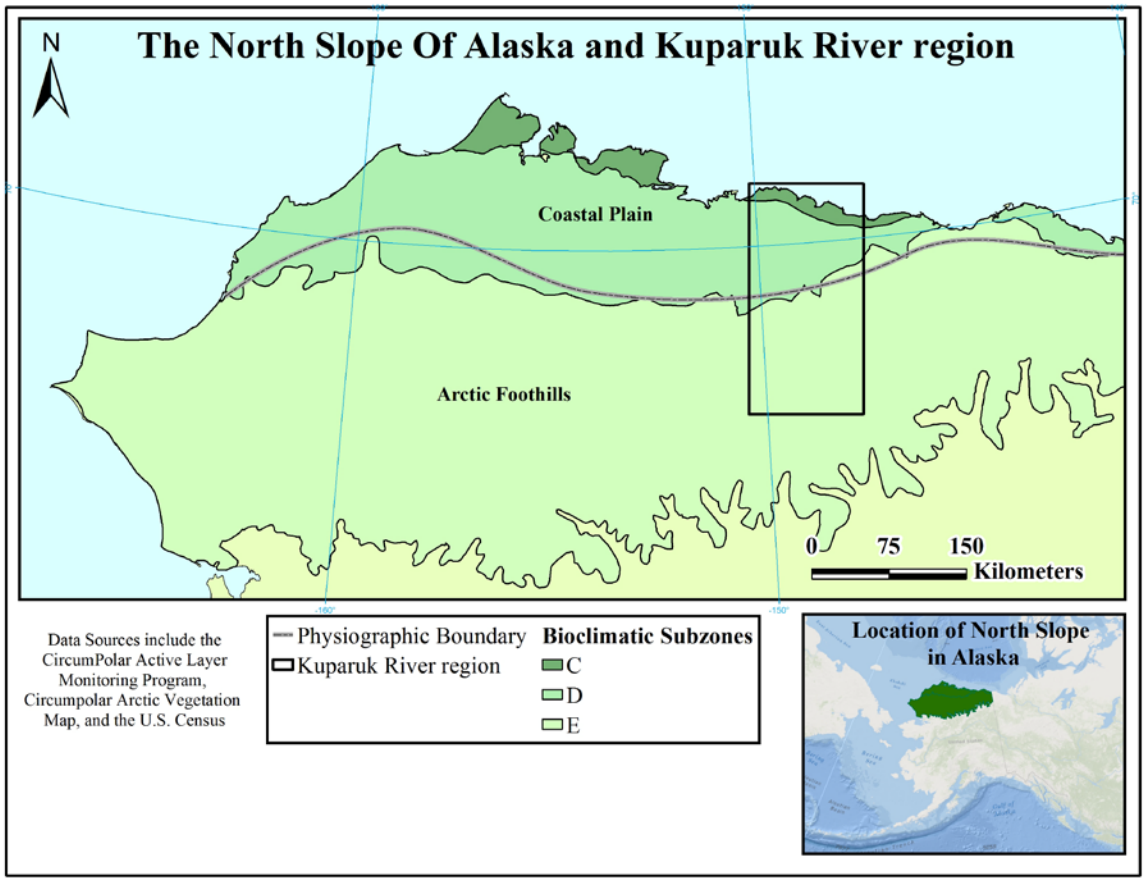

III.2 Study Sites

Nine 1-hectare Flux Study plots were used in this study and these sites are located in bioclimatic subzones D and E (Fig. III-2). Data on these sites were gathered as part of the Circumpolar Active Layer Monitoring program (CALM), which includes these sites as well as additional larger and smaller plots around the world (Shiklomanov et al., 2012). These nine Flux Study plots are referred to as the CALM study sites throughout the text, but these 9 were the only CALM sites for which these dispersed soil-surface

temperature data were available. All the included CALM sites located in subzone D are also located on the Arctic coastal plain, while all sites located in subzone E are also located in the foothills province. Characteristics of the nine CALM study sites utilized for this study are shown in Table III-1.

Subzone D contains three CALM sites with the distributed soil-surface temperature records (U7b, U7c and U31) and is comprised of moist and wet non-acidic tundra at sites U7b and U7c, and wet tundra at site U31. Sites U7b and U7c are located on drained lake basins on the outer coastal plain, while site U31 is located on the inner coastal plain about 64 km south of sites U7b and U7c. Subzone E contains the other six CALM sites with the distributed soil-surface temperature records (U32a, U32b, U12b, U11b, U11c, and U10), and these sites are located in both the foothills province. These sites have more complex vegetation patterns than the sites in subzone D and have representatives of both, moist acidic and nonacidic tundra. Sites U32a and U32b are located in the northern arctic foothills and are non-acidic tundra, respectively, while site U10 is a complex of shrubs and water track. Sites U12b, U11b, and U11c, are located in the southern foothills, and are a moist non-acidic and water-track complex, wet non-acidic and moist non-acidic sites, respectively. Figure III-2 displays the locations of CALM sites in the study area. Despite the similarity in topography and vegetation within each physiographic province and subzone, these features can vary locally. Thus, sites within the same subzone and physiographic region may experience significant differences in soil-surface temperatures and snow-cover characteristics.

Table III-1 Characteristics of the nine CALM sites used in this study.

CALM Site	Land-Cover Class	Elevation (m)	Soil Type (highest %)	Orientation and Slope
Coastal Plain				
U7b	Moist Nonacidic	12	Pergelic cryoborolls	Flat
U7c	Wet Nonacidic	12	Histic pergelic cryaquolls	Flat
U31	Wet Tundra	349	Pergelic cryorthents	Flat
Foothills				
U32a	Moist Nonacidic	269	Pergelic cryaquolls	NW 4
U32b	Moist Acidic	360	Pergelic cryaquepts	Flat
U12b	Moist Acidic/Water Track complex	777	Pergelic cryaquepts	N 3
U11b	Wet Acidic	917	Histic pergelic cryaquolls	N 1
U11c	Moist Acidic	938	Pergelic cryaquepts	W 15
U10	Shrubs / Water Track complex	537	Histic pergelic cryaquolls	SE 4

Figure III-2 Location of the CALM study sites in the Kuparuk region utilized in this study. Bioclimatic subzones and physiographic boundaries are shown.

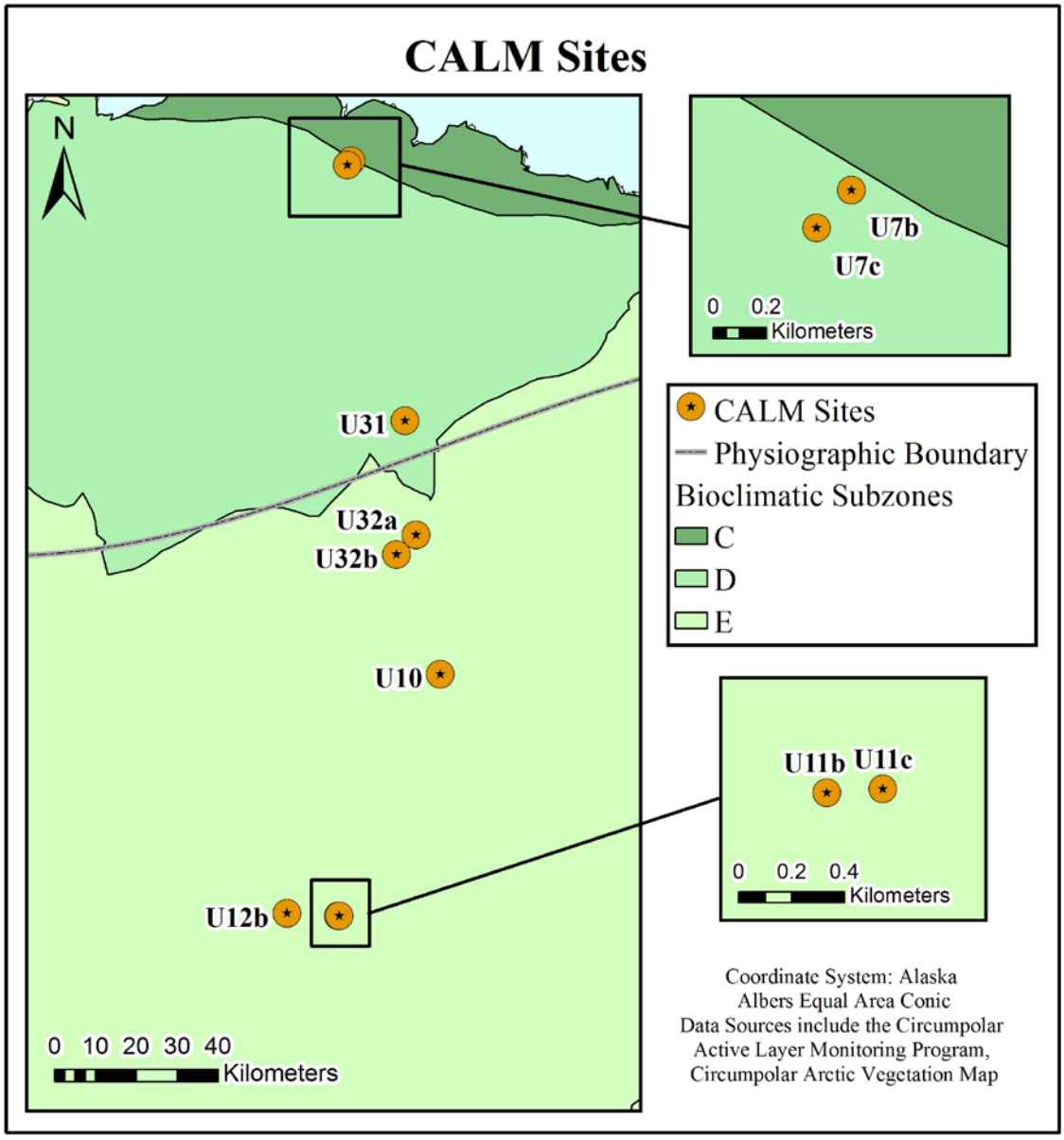

IV. Air and Soil-Surface Temperature Observations

IV.1 Introduction

Understanding the spatial and temporal variability of temperature in the Arctic is necessary to infer possible regional impacts to ecosystems. Both air and soil-surface temperatures vary spatially across the watershed. The spatial variability of air temperature relies primarily upon two factors: topography in the foothills, and continentality on the coastal plain (Shiklomanov and Nelson, 2003). Soil-surface temperatures in high latitudes are impacted by air temperatures and are also dependent upon microclimatic factors such as snow cover, vegetation, and soil moisture (Klene et al., 2001b), which results in much higher heterogeneity between sites.

Past climate studies document increasing global air temperatures, which will likely pose a significant impact on snow cover in the Arctic region (Callaghan, 2011b). The Kuparuk region exhibits diverse climatic conditions as a result of its extent and complex terrain (Shiklomanov and Nelson, 2003). This chapter analyzes long-term air and soil-surface temperature observations at CALM sites in the Kuparuk to quantify trends and variability of air and soil-surface temperatures between sites. These results will be compared to snow characteristics in later chapters.

IV.2 Background

IV.2.1 General Temperature Trends on the Alaskan North Slope

While there is limited information on soil-surface temperature trends from past studies on the North Slope, long-term air temperature trends have been examined. Mean annual air temperatures on the Alaskan North Slope are below -10 °C and only three months (June to August) have mean air temperatures above the freezing point (Wendler et al., 2010). According to Wendler et al. (2010), air temperatures on the coastal portion of the North Slope are relatively homogenous. A recent study that covered a 36-year time period (1997 to 2007) found a significant warming of 2.9 °C at Barrow, the northernmost point of Alaska and this warming was most pronounced during the winter season (Wendler et al., 2010). Stieglitz et al. (2003) fount that air temperatures at Barrow have warmed 1°C over a 60-year time period (1940 to 2000) and 3 °C over a 30-year time period (1970 to 2000). In the Kuparuk region, records of the mean, minimum and maximum air temperatures from 1995 to 2006 showed a slight decline in mean and maximum annual air temperature for the coastal plain and in maximum annual air temperature for the foothills (Streletskiy et al., 2008). Overall, observed changes in air temperature trends on the North Slope vary depending upon the location and period included. Observed trends that cover at least a 30-year time period indicate warming on the North Slope.

IV.2.2 Spatial Variability of Air Temperatures in the Kuparuk Region

Past studies in the Kuparuk Region have found mean annual air temperatures to increase from north (subzone D) to south (subzone E). This is attributable to the moderating effect of the Arctic Ocean, which keeps air temperatures near the freezing point. Annual air temperatures in the foothills are warmer because of a transition from a maritime to continental climate (Streletskiy et al., 2008; Nyland et al., 2012). Results from a study by Klene et al. (2008) showed that ten-year mean air temperatures in the Kuparuk region from February and July ranged from -18.3 °C to -28.2 °C and 7.3 °C to 10.8 °C, respectively. In a study by Shiklomanov and Nelson (2003), air temperature in the coastal plain was found to be related to continentality because of the low relief, while complex topography in the foothills dominated air temperatures there. The coldest summer air temperatures were measured at the southernmost sites in the high mountains of the northern Brooks Range, where temperatures remain close to 0 °C during the summer (Shiklomanov and Nelson, 2003).

IV.2.3 Variability of Soil-Temperatures in the Kuparuk Region

Unlike air temperatures, soil-surface temperatures are highly variable because they are influenced by vegetation, snow cover, and soil moisture (Streletskiy et al., 2008; Klene et al., 2001b; Nyland et al., 2012). These factors cause soil-surface temperatures to exhibit much greater spatial variability than air temperatures, and in northern Alaska soil-surface temperatures should be consistently colder than air temperatures in the summer and warmer than air temperatures in the winter, due to the insulating effects of

vegetation and snow. Vegetation cools the soil-surface during the summer by providing shade, which helps to reduce soil-temperatures and the summer thaw propagation. In winter, snow's low thermal conductivity keeps soil-surface temperatures warmer than air temperatures. In the Kuparuk region, the differences between air and soil-surface temperatures were found in the shrublands and moist acidic tundra (Klene et al., 2011b; Nyland et al., 2012; Streletskiy et al., 2008).

During the summer, research found soil-surface temperatures to be warmer in areas that lacked vegetation such as the top of hills and mountains, and along streams in the Kuparuk (Klene et al., 2001b; Nyland et al., 2012; Streletskiy et al., 2008). These exposed surfaces of sand, gravel, and bedrock have no shading, have less evaporation, and warmer ground thermal regimes. Along with vegetation and snow, Klene et al. (2001b) found soil moisture to impact soil-surface temperatures. Plants and mosses of moist acidic tundra in the Kuparuk region shade the underlying ground and provide a thick insulation layer, which can limit evaporation. The increased water available in these types of soil lowers the heat absorbed into the ground (Klene et al., 2001b).

Previous studies have utilized n-factors to observe the effects of vegetation and snow on the ground thermal regime (Klene et al., 2008; Streletskiy et al., 2008). A description of n-factors can be found in Chapter VI of this thesis. Cooler summer soil-surface temperatures were recorded in the foothills physiographic province, while warmer soil-surface temperatures were found on the coastal plain. This variation in surface temperatures from north to south was a result of the increase in density of the vegetation cover in the foothills (Streletskiy et al., 2008). Similarly, Klene et al. (2008) calculated winter n-factors and found southern sites with deeper snow experienced more

insulation than northern sites. Being that snow accumulation is influenced by vegetation, ground temperatures were found to be dependent upon both snow depth and vegetation (Klene et al., 2008).

IV.3 Methodology

IV.3.1 Data Availability

This study focuses on nine CALM sites, which have been collecting continuous air and distributed soil-surface temperature observations since 1995. These sites are arranged along a north-south climatic gradient within the Arctic coastal plain and foothills and exhibit differences in continentally and topography. Each site was instrumented with Hobo®[1] portable data loggers connected to probe-type thermistors. The temperature range for each logger/thermistor system was -50 °C to 33 °C and the resolution was approximately 0.32 °C. At each site, one thermistor was placed in a radiation shield approximately 2 meters above the ground surface, and thermistors were placed at the soil surface interface in a range of micro-topographic locations to capture the spatial variability of soil-surface temperatures within each 1-ha plot. Temperature measurements were collected at either 1 or 2-hour intervals daily. The data was downloaded annually, and details on the methodology are provided in Klene et al. (2001a). Additional temperature observation sites that are also part of the CALM network on the North Slope of Alaska (Deadhorse, Tarn Road, Spine Road, Happy Valley, Imnavait, Galbraith Ridge, and Galbraith Lake)

[1] Produced by Onset Computer Corporation®, Bourne, MA. Stowaway, Hobo Pro, and Hobo Pro v2 dataloggers have been used over the course of the study.

collected air and/or soil-surface temperature data. These sites are included in this chapter's temperature analysis to obtain a more accurate estimation of temperature trends during the study period.

Figure IV-1 Location of CALM study sites used to observe air and soil-surface temperatures. Additional temperature observation sites, bioclimatic subzones and the physiographic boundary are shown.

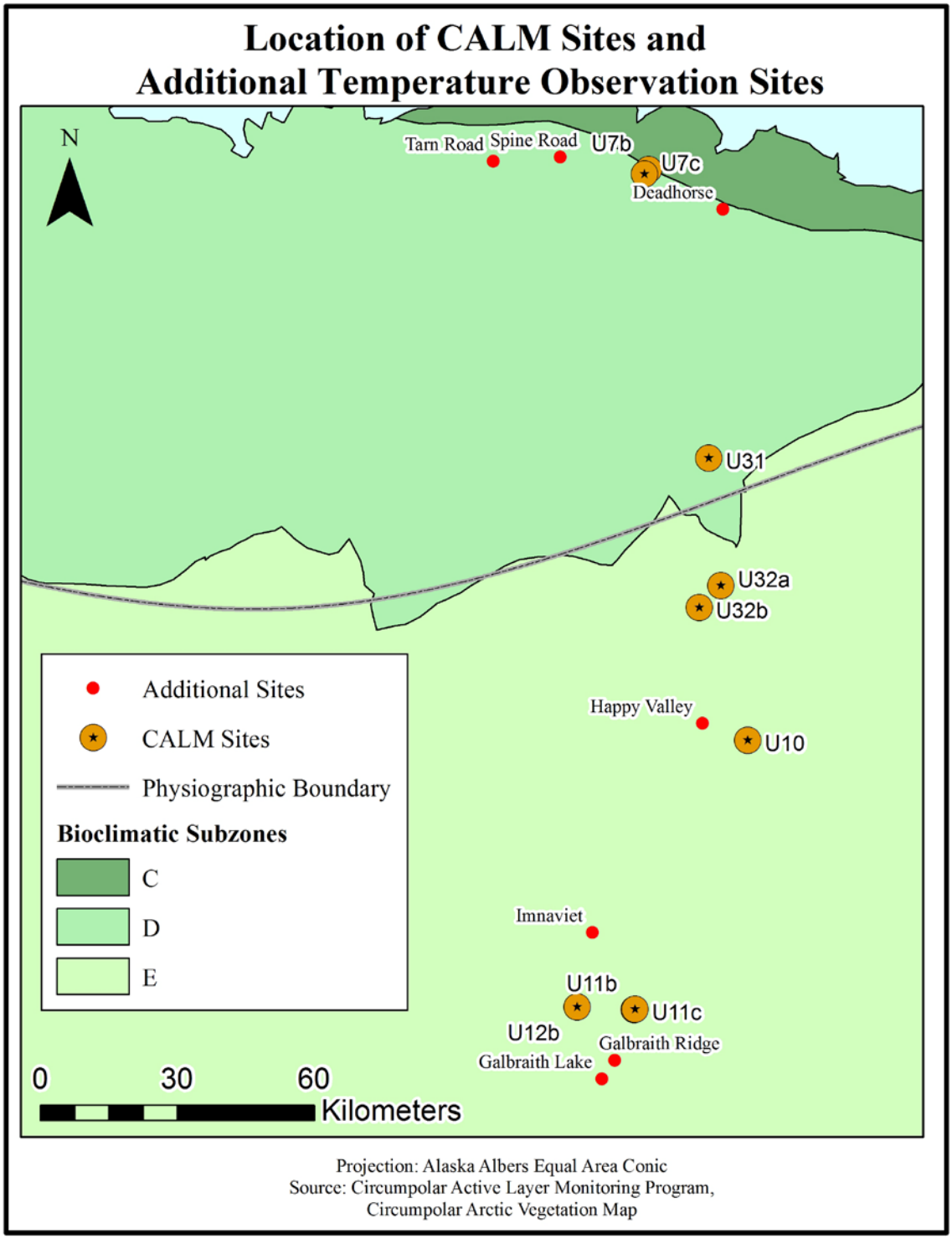

IV.3.2 Data Analysis

Hourly and bi-hourly air temperatures were averaged into daily and monthly air temperatures at each CALM study site. Monthly air temperatures were then averaged to obtain mean summer (June to August) and winter (December to February) air temperatures. Monthly air temperatures were also averaged into hydrologic years, which are measured from September 1 to August 31. Hydrologic years were used in this study to access annual temperature trends because they allowed for the inclusion of the entire snow-cover period in one year. The annual, summer, and winter air temperatures were averaged to get the aggregate of subzones D (U7b, U7c, U31) and E (U32a, U32b, U12b, U11b, U11c, U10). Air temperatures from additional observation sites were also included (subzone D = Tarn Road, Spine Road and Deadhorse; subzone E = Happy Valley, Imnavait Creek, Galbraith Ridge, and Galbraith Lake) in the appropriate subzone.

Similarly, hourly and bi-hourly soil-surface temperature measurements were calculated into daily and monthly means. Monthly soil-surface temperatures were averaged into mean summer and winter temperatures. The monthly soil-surface temperatures were also averaged by hydrologic years to obtain annual soil-surface temperatures. The data for annual, winter, and summer soil-surface temperatures were averaged to get the aggregate for subzones D and E. Additional soil-surface temperature observation sites were also included (subzone D = Tarn Road and Spine Road; subzone E = Imnavait Creek, Galbraith Ridge, and Galbraith Lake) within the appropriate subzones.

IV.4 Results

IV.4.1 Spatial Variability of Observed Air Temperatures

Annual, summer, and winter air temperatures were generally colder at northern sites in subzone D (U7b, U7c, and U31) and warmer at southern sites in subzone E (U32a, U32b, U12b, U11b, U11c, and U10; Figure IV-2). Sites U7b, U7c, and U31 experienced the coldest annual air temperatures during the study period and temperatures were relatively similar each year at these sites (Figure IV-2a). The low relief of the coastal plain allows temperatures at these sites to remain relatively uniform and thus, temperatures on the coastal plain are strongly dependent on continentally (Shiklomonav and Nelson, 2003). Site U11c had the warmest annual air temperatures and was on average -7.0 °C. The mean variability of annual air temperatures was about 4.0 °C each year between all study sites.

According to Figure IV-2b, sites U7b and U7c experienced the coldest summer air temperatures, while all other study sites were slightly warmer. The mean annual range in summer air temperatures between study sites was 3.8 °C. During the winter, site U31 experienced the coldest air temperatures, with a mean of -27.1 °C (Figure IV-2c). While site U11c had the warmest winter air temperatures of all the sites. The average range in winter air temperatures between study sites was about 8.0 °C each year.

Figure IV-2 Mean annual (a), summer (b), and winter (c) air temperatures observed at study sites between 1996 and 2013.

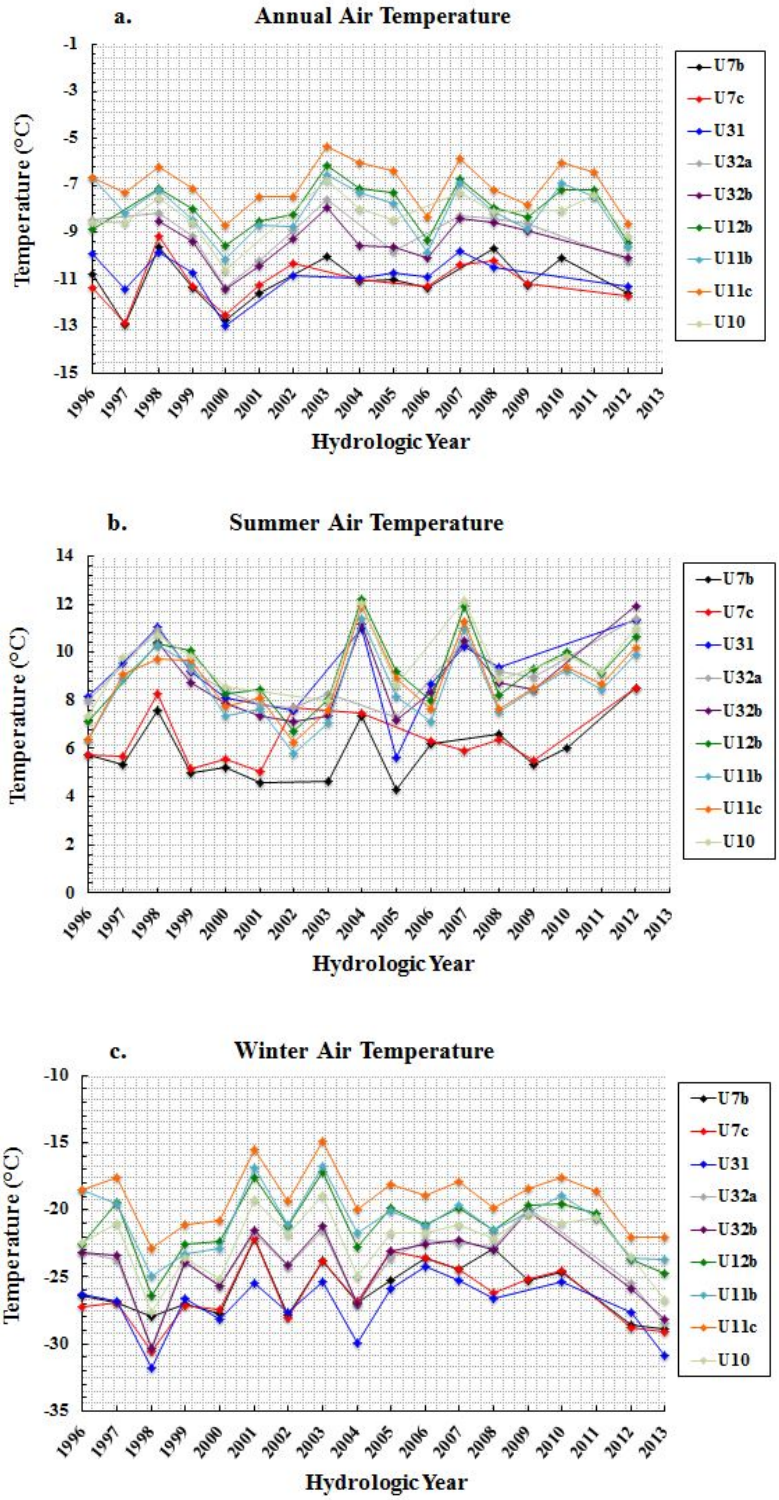

According to Table IV-1, mean annual air temperatures were colder in subzone D than E. Mean annual air temperatures were -11.0 °C in subzone D, while the mean temperature was -8.3 °C in subzone E. Mean summer and winter air temperatures were also colder in subzone D, 7.2 °C and -26.4 °C, respectively. These colder air temperatures are attributable to the adjacency of subzone D to the cold Arctic Ocean, which leads to cooler summer air temperatures. During the winter, the sea ice keeps temperatures along the coast colder by creating a continental effect rather than a maritime (Hall et al., 1986). The coldest winter air temperatures were experienced at site U31 on the coastal plain, the most continental out of the sites in subzone D. Overall, sites in both subzones experienced winter temperatures less than -19.0 °C and subzone D experienced the coldest temperatures.

Table IV-1 Mean annual, summer, and winter air temperatures observed at study sites between 1996 and 2013.

Mean Air Temperature (°C) (1996 - 2013)			
Site	**Annual**	**Summer**	**Winter**
Subzone D			
U7b	-11.1	5.9	-25.9
U7c	-11.1	6.4	-26.2
U31	-10.8	9.2	-27.1
Average	-11.0	7.1	-26.4
Subzone E			
U32a	-9.1	9.0	-24.1
U32b	-9.4	8.9	-24.1
U12b	-7.9	9.2	-21.2
U11b	-8.1	8.5	-20.9
U11c	-7.0	8.7	-19.1
U10	-8.2	9.7	-22.4
Average	-8.3	9.0	-22.0

IV.4.2 Temporal Variability of Observed Air Temperatures

According to Figure IV-3a, mean annual air temperatures observed in subzone D were essentially stable, increasing by 0.0 °C per year during the study period and were on average -10.7 °C. Maximum temperatures decreased 0.1 °C per year, while minimum temperatures increased 0.1 °C per year. The range between maximum and minimum air temperature was very small, especially from 2009 to 2013. The mean range between maximum and minimum annual air temperatures in subzone D was 1.6 °C each year.

Summer air temperatures in subzone D remained steady during the study period with a mean summer air temperature of 7.1 °C (Figure IV-3b). Maximum summer air temperatures decreased 0.0 °C per year, while minimum temperatures increased 0.1 °C per year. The mean range between maximum and minimum summer temperatures was 3.4 °C.

Similarly, winter air temperatures also remained steady throughout the study period in subzone D (Figure IV-3c). The minimum temperatures increased by about 0.1 °C per year and maximum temperatures decreased 0.2 °C per year. The mean winter temperature for the study period was -26.0 °C, and the mean minimum and maximum temperatures were -27.2 and -24.1 °C. The mean range between the mean minimum and maximum winter temperatures was 3.1 °C each year. Overall, air temperatures appear to be remaining steady in subzone D, with mean air temperatures increasing only slightly.

Figure IV-3 Mean annual (a), summer (b), and winter (c) air temperatures in subzone D between 1996 and 2013.

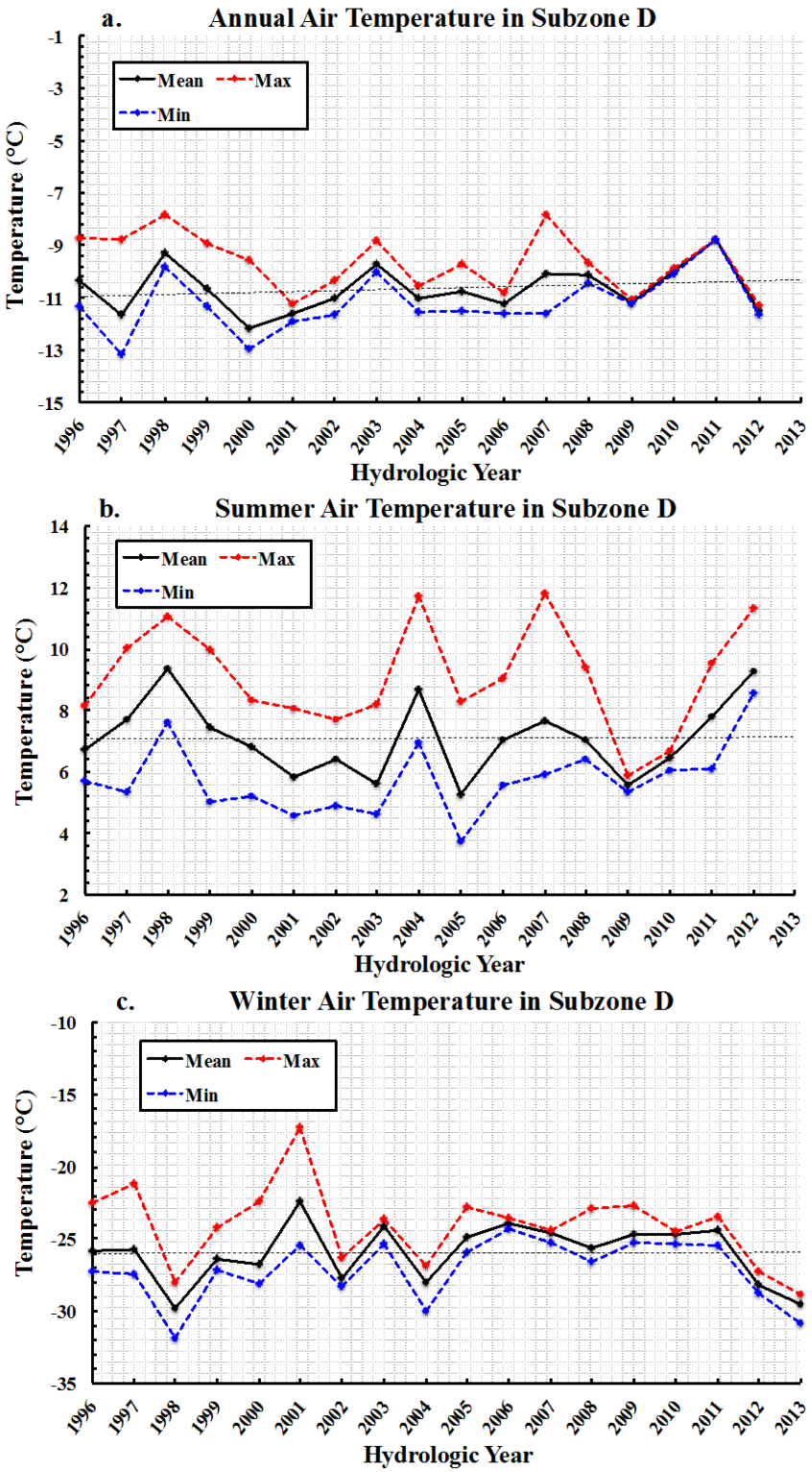

Mean annual air temperatures in subzone E increased 0.0 °C per year and were on average -8.1 °C during the study period (Figure IV-4a). Minimum annual air temperatures increased 0.0 °C and maximum temperatures increased 0.1 °C per year. Overall, mean annual air temperatures were about 3.0 °C warmer in subzone E than D. The range between mean maximum and minimum annual air temperatures in subzone E was not very large between sites, and was on average 2.8 °C.

Mean summer air temperatures increased 0.1 °C per year and were on average 8.9 °C (Figure IV-4b). Minimum and maximum summer air temperatures also increased by 0.1 and 0.1 °C per year. Mean summer air temperatures in subzone E increased at a faster rate than those in subzone D and were slightly warmer each year during the study period. The mean range between summer mean maximum and minimum air temperatures was about 1.7 °C in subzone E each year.

Winter air temperatures in subzone E increased slightly by 0.1 °C per year during the study period (Figure IV-4c). Minimum winter temperatures increased 0.1 °C per year and maximum temperatures increased 0.2 °C per year. The mean winter air temperature was -21.5 °C, and the mean minimum and maximum temperatures were -24.1 °C and -17.9 °C, respectively. The mean range between minimum and maximum winter temperatures was 6.3 °C in subzone E, which is about twice the range of subzone D. The greater range in winter air temperatures in subzone E may be attributable to topography. Overall, mean winter air temperatures in subzone E were warmer than those in subzone D by about 4.0 °C each year and experienced greater variation between sites.

Figure IV-4 Mean annual (a), summer (b), and winter (c) air temperatures observed in subzone E between 1996 and 2013.

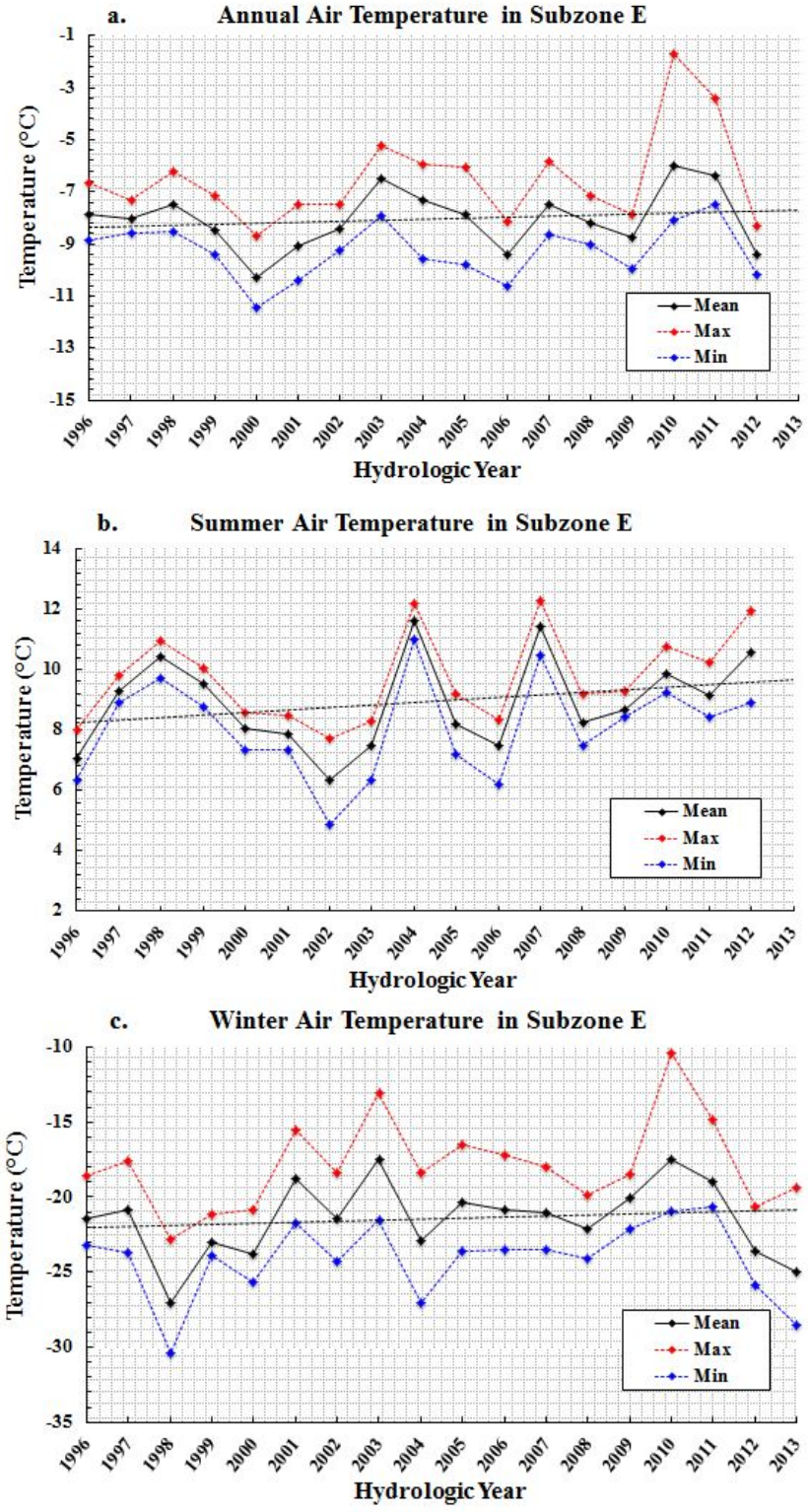

IV.4.3 Spatial Variability of Observed Soil-surface Temperatures

According to Figure IV-5a, the coldest mean annual soil-surface temperatures were experienced at site U7b. While sites U31, U11b, and U10 experienced the warmest annual soil-surface temperatures. The mean range between mean annual soil-surface temperatures at all study sites was 5.0 °C each year. Sites U11b and U31 had some of the warmest summer soil-surface temperatures (Figure IV-5b), while sites U7b, U12b, U11c, and U10 had the coldest. The mean range between summer soil-surface temperatures was about 3.0 °C each year.

The coldest winter soil-surface temperatures occurred at sites U7b and U7c on the coastal plain (Figure IV-5c), while the warmest winter soil-surface temperatures occurred at sites U10, U11b, and U31. The mean range in winter soil-surface temperatures during the study period was about 10.2 °C each year, which is more than twice the range of soil-surface temperatures experienced annually and during the summer.

Figure IV-5 Mean annual (a), summer (b), and winter (c) soil-surface temperatures observed at study sites between 1996 and 2013.

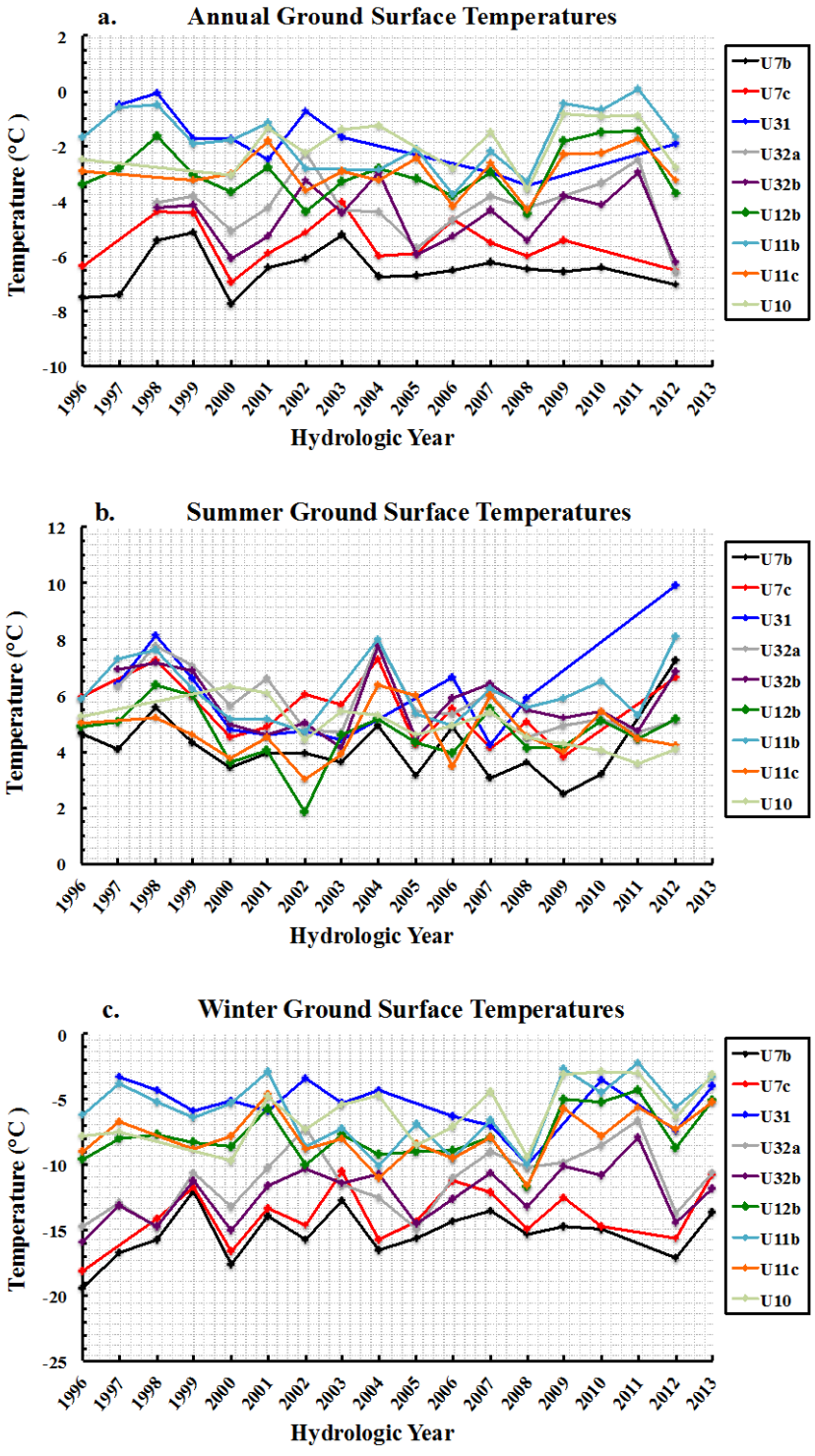

Table IV-2 displays mean annual, summer, and winter soil-surface temperatures observed at study sites between 1996 and 2013. The mean annual soil-surface temperature at study sites in subzone E was -3.1 °C, which was warmer than subzone D (-4.6 °C). Summer soil-surface temperatures were very similar in both subzones, even though summer air temperatures were generally warmer in subzone E. The summer soil-surface temperatures in subzone E may be cooled by the greater vegetation density, which provides greater shading of the underlying ground.

There is high variability in winter soil-surface temperatures between sites during the study period. This variability may be caused by micro-scale differences in vegetation, snow cover, topography, and soil conditions. Winter soil-surface temperatures were generally warmer in subzone E than subzone D in winter and in terms of mean annual temperatures. An exception is site U31 in subzone D, which had the warmest winter soil-surface temperature of the sites examined. This may be attributable to a thick snow cover at site U31. Overall, subzone E has warmer winter soil-surface temperatures, which may be caused by greater snow depths that accumulate there. The flat topography, lower vegetation density, and frequent winds limit the snow holding capacity of subzone D.

Table IV-2 Mean annual, summer, and winter soil-surface temperatures observed at study sites between 1996 and 2013.

Mean Soil-surface Temperature (°C) (1996 to 2013)			
Site	**Annual**	**Summer**	**Winter**
Subzone D			
U7b	-6.5	4.1	-15.3
U7c	-5.5	5.5	-13.8
U31	-1.7	6.0	-5.4
Average	-4.6	5.2	-11.5
Subzone E			
U32a	-4.2	5.7	-11.2
U32b	-4.6	5.7	-12.2
U12b	-3.0	4.6	-7.8
U11b	-1.7	6.1	-5.9
U11c	-2.9	4.7	-7.9
U10	-1.9	4.9	-5.9
Average	-3.1	5.3	-8.5

IV.4.4 Temporal Variability of Observed Soil-surface Temperatures

The mean annual soil-surface temperature in subzone D was -5.2 °C, with means showing a decreasing trend of 0.1 °C per year, as shown in Figure IV-6a. Minimum soil-surface temperatures remained constant and display the lowest value in 2008. This low was attributable to low soil-surface temperature measurements at Spine Road. Maximum temperatures show a decrease of 0.2 °C per year. The mean range between minimum and maximum annual soil-surface temperatures during the study period was 3.3 °C.

According to Figure IV-6b, summer soil-surface temperatures decreased 0.1 °C per year in subzone D. The mean summer soil-surface temperature during the study period was 4.9 °C. Maximum summer soil-surface temperatures decreased 0.0 °C and minimum ground surface temperatures decreased 0.1 °C per year. The mean range between summer soil-surface temperatures was about 2.0 °C each year.

The mean winter soil-surface temperature in subzone D was -12.5 °C and it increased 0.0 °C during the study period, as shown in Figure IV-6c. Winter soil-surface

temperatures at site U31 were the warmest and were on average -5.4 °C during the winter. All other sites in subzone D had mean winter soil-surface temperatures between -13.0 and -16.0 °C, and the coldest minimum temperature was -26.2 °C recorded at Spine Road in 2008. The mean range of winter soil-surface temperatures in subzone D was 8.5 °C, which is more than twice the range of winter air temperatures in subzone D. Overall, soil-surface temperatures in subzone D showed slight changes each year during the summer and winter. The range between maximum and minimum soil-surface temperatures was substantially greater during the winter season in subzone D.

Figure IV-6 Mean annual (a), summer (b), and winter (c) soil-surface temperatures observed at study sites between 1996 and 2013.

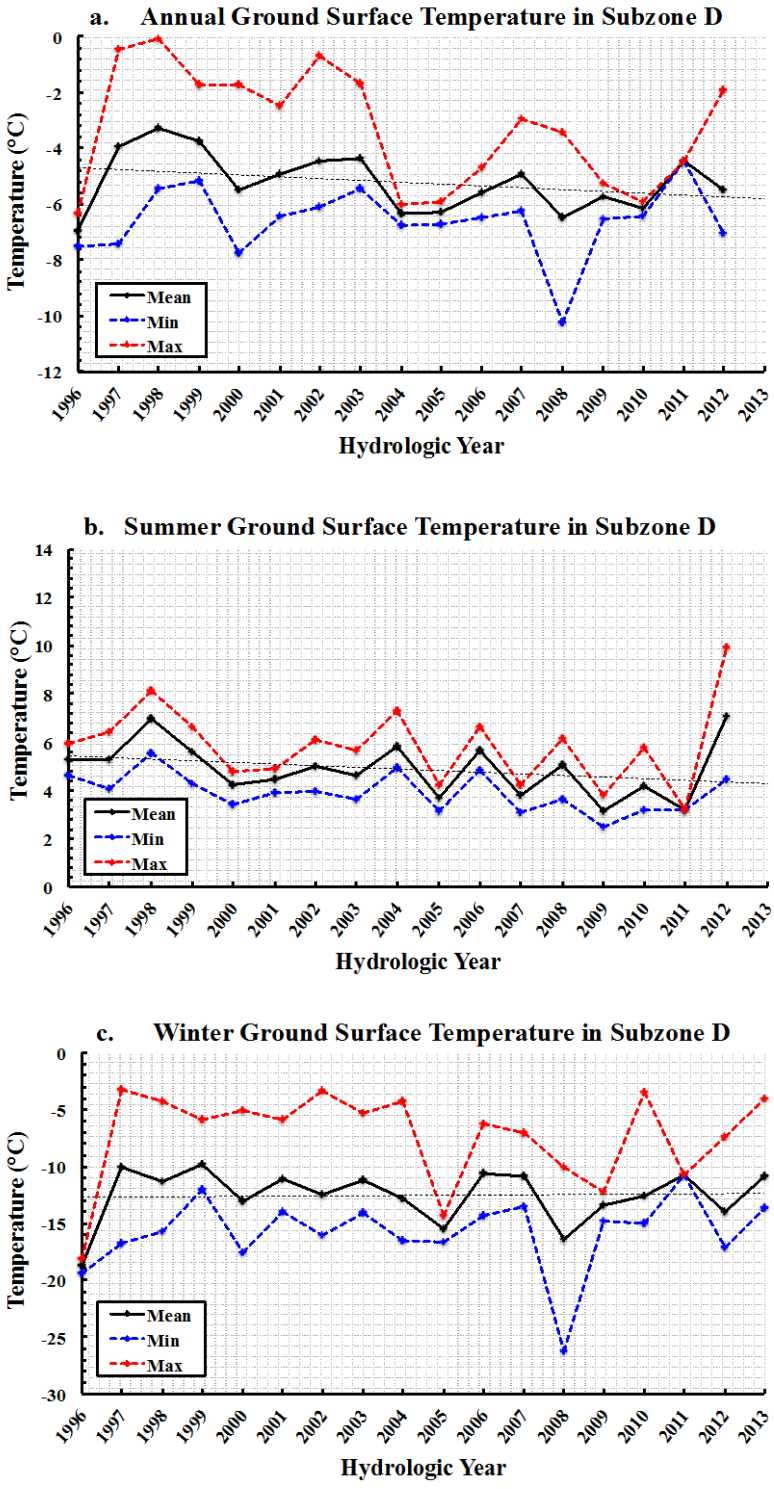

According to Figure IV-7a, annual soil-surface temperatures in subzone E decreased 0.0 °C during the study period and the average mean was -3.2 °C. Maximum annual temperatures remained constant, while minimum temperatures decreased 0.1 °C per year. The mean range between maximum and minimum annual soil-surface temperatures in subzone E was 3.6 °C. Overall, annual soil-surface temperatures in subzone E were warmer than those in subzone D by about 2.0 °C and both subzones experienced similar ranges between maximum and minimum soil-surface temperatures.

Summer soil-surface temperatures in subzone E remained steady during the study period, as shown in Figure IV-7b. The mean summer soil-surface temperature was 5.5 °C. Maximum summer soil-surface temperatures increased 0.1 °C per year, while minimum soil-surface temperatures decreased 0.0 °C. The peak maximum summer soil-surface temperature of 12.1 °C in 2004 occurred at Imnavait. The mean range of summer soil-surface temperatures was 3.5 °C.

The winter soil-surface temperature in subzone E was -9.3 °C, and this mean increased 0.1 °C per year (Figure IV-7c). Maximum winter ground temperatures increased 0.1 °C per year, while minimum temperatures decreased 0.1 °C per year. The minimum temperature hit a peak low in 2004 at -19.4 °C, and this was attributable to cold ground temperatures recorded at Imnavait. Overall, winter soil-surface temperatures in subzone E were warmer than those in subzone D by about 3.0 °C. The mean range between the maximum and minimum winter soil-surface temperature was 9.8 °C, which is greater than the range observed between soil-surface temperatures annually and during the summer in subzone E. This range is also greater than the range of winter air temperatures in subzone E. Hence, soil-surface temperatures exhibit greater spatial

variability than air temperatures and this variability is significantly greater during the winter.

Figure IV-7 Annual (a), summer (b), and winter (c) soil-surface temperatures observed in subzone E between 1996 and 2013.

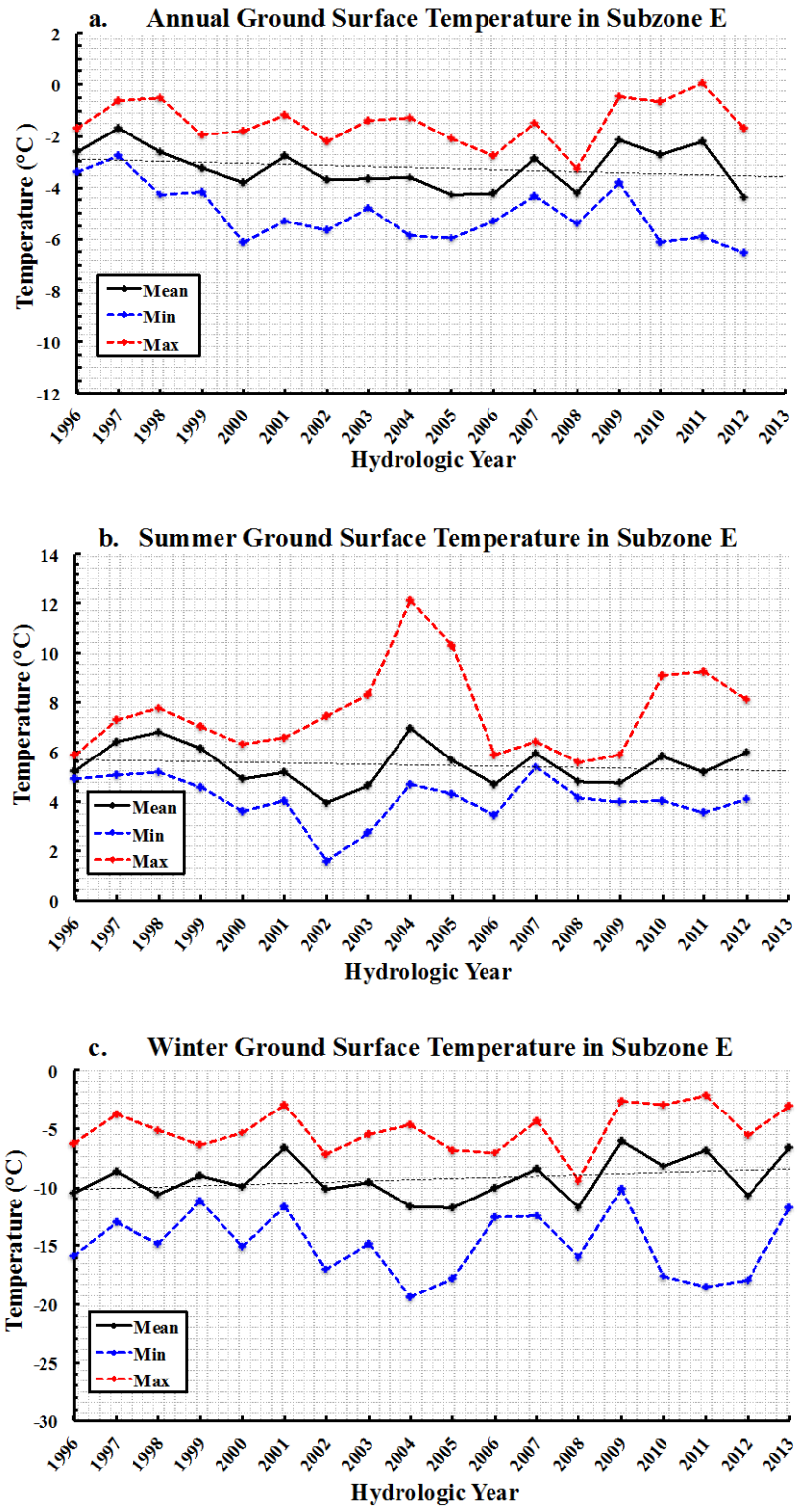

IV.5 Conclusions

While numerous studies indicated increasing air temperatures in the Arctic, observations of air temperatures at CALM study sites indicated little to no change during the study period. CALM has only been collecting temperature data since 1995 and thus, it is concluded that an insufficient amount of data is available to determine trends in air and soil-surface temperatures.

However, the spatial variability of air and soil-surface temperatures could be analyzed. Soil-surface temperatures in the study area were found to show substantially greater variability between sites than air temperature, especially during the winter. The mean range of winter soil-surface temperatures was more than twice the range of summer and annual soil-surface temperatures in both subzones. Hence, the high variability of soil-surface temperature during the winter may be linked to factors not present during the summer months, specifically snow cover. Subzone E recorded warmer soil-surface temperatures than subzone D, and this may indicate greater snow depths in the subzone. The relation between soil-surface temperature variability and snow-cover characteristics will be discussed in the following chapters.

V. Snow-Cover Characteristics

V.1 Introduction

Snow cover plays a key role in the Earth's energy balance by acting as an insulator, keeping underlying soil-surface temperatures warmer than the ambient air (Calonne et al., 2011; Sturm et al., 2005). The Arctic tundra is covered with snow for approximately two-thirds of the year, with snow increasing slowly through much of the winter. Snowmelt is comparatively very quick and can be as little as 5 days in the spring (Sturm et al., 2005). However, changing climatic conditions are expected to cause the timing of seasonal snowmelt to become earlier in the spring (Callaghan et al., 2011a; Callaghan et al., 2011b).

Snow cover in the Arctic is extremely variable and can be relatively thin, with snow drifting in some places and being blown from others. The high spatial variability of snow cover makes it difficult to monitor, especially using point-based observation networks with large gaps (Callaghan et al., 2011a). A methodology to monitor snow characteristics daily that is inexpensive and covers as large of a spatial area as possible is highly desirable by Arctic research scientists. This chapter discusses the use of observed air and soil-surface temperatures, precipitation and snow-depth data, and images taken using digital cameras, to estimate snow-cover duration (SCD) and snow depth at a series of sites located in different bioclimatic and physiographic regions in Arctic Alaska.

V.2 Background

V.2.1 Changes in Snow-Cover Characteristics

Evidence from the past shows that SCD in the Arctic has been decreasing, while the total amount of snow accumulation in some areas has been increasing (McBean, 2005). According to a study by Olsen et al. (2011), seasonal SCD in the Arctic is expected to decrease about 10-20 % by the year 2050. Alaska and other maritime locations are experiencing the largest decreases in SCD of ~30-40%, according to global climate models (Callaghan et al., 2011a). Callaghan et al. (2011a) stated that the decrease in SCD is mostly attributable to an earlier snowmelt rather than a later snow onset. A decrease in SCD by about 3 days per decade in the Alaskan-Canadian sector of the Arctic has been observed. It was found using the National Oceanic and Atmospheric Administration's (NOAA) satellite record that Arctic SCD changed by about -0.49 days per decade for the snow-cover onset period, and -3.43 days for the snow-cover melt period. These changes in winter SCD are likely attributable to changes in temperature and precipitation (Callaghan et al., 2011a).

A decreasing SCD will expose the dark underlying surface and promote surface heating. This will lead to an earlier convective precipitation regime in the Arctic (Callaghan et al., 2011b). According to a past study by Callaghan et al. (2011a), climate stations located north of 60°N in all areas of the Arctic have experienced an increase in cold season precipitation from between 1936 and 2009. McBean (2005) claimed that Arctic precipitation is increasing by about 1% per decade. Annual precipitation in the region is predicted to increase an average of 9-25% by 2099 (Clilverd et al., 2011).

Temperature and precipitation increases in the Arctic will likely promote the occurrence of winter freeze/thaw cycles, and these cycles are becoming more common as more winter precipitation falls as rain rather than snow (Clilverd et al., 2011). These winter freeze/thaw cycles quicken the rate of snowmelt and have an impact on snow stratigraphy by increasing layers of ice at the top and within the snowpack (Callaghan et al., 2011a).

Snow cover plays a critical role in the Arctic's annual energy balance and as a result, changes in snow-accumulation trends would have a crucial impact on the Arctic region. Snow is the most reflective surface on Earth and fresh snow has an albedo of about 80-90% (Callaghan et al., 2011b). The high albedo of snow provides a cooling effect for the Arctic and the rest of the globe by reflecting a large percentage of shortwave radiation rather than absorbing it (Oke, 1978). As snow ages and becomes darker, snows albedo decreases as a consequence of an increase in water content and impurities such as dust particles (Oke, 1978; Schmidt et al., 2009). A study by Adams et al. (2011) demonstrated the effect of snow reflectivity by measuring the temperature difference between snow-covered trees and snow-free trees on a snow-covered slope. Snow on the slope with snow-covered trees was found to be colder than snow in areas of snow-free trees, and experienced 18% less sublimation than snow on the slope with snow-free trees (Adams et al., 2011). As snow cover continues to decline, the rate of decreasing SCD will likely continue to increase because of higher temperatures.

V.2.2 Importance of Snow

The insulation provided by snow limits deep freezing of the ground by keeping ground temperatures warmer. Thus, snow depth has a strong influence on the active layer and permafrost, especially near the southern permafrost limit (Callaghan et al., 2011b). Areas are likely to have continuous permafrost if they have a very thin snow cover, or if they remained snow free and have freezing temperatures (French 2007; Morse et al., 2012), whereas areas with deep snow cover are associated with discontinuous or no permafrost. The active layer in these areas may not be able to freeze in the winter if the snow depth or soil moisture is great enough. If this happens, less energy and time will be spent thawing the active layer in the following summer and more energy can be spent on thawing the underlying permafrost (Morse et al., 2012).

The growth of Arctic vegetation can also be promoted by snow cover, which keeps the underlying ground from freezing so it stays nutrient rich (Bonfils et al., 2012, Sturm et al., 2005). The ability of snow to keep soil warm stimulates soil microbial activity and the mineralization of nitrogen, which is used for plant growth. This rich soil is used for the next growing season and as a result, a more robust cycle of plant growth is formed (Sturm et al., 2005). Snow also protects vegetation from extreme low temperatures, large temperature fluctuations, and desiccation. Vegetation that remains covered with snow during the winter is usually able to flourish and re-bud quickly in the spring (Bonfils et al., 2012).

V.2.3 Snow Accumulation

The extreme spatial variability of snow cover in the Arctic is mostly attributable to changes in topography and vegetation. The deepest snow is found in areas with the tallest and densest shrubs, which hold snow in place and reduce sublimation (Morse et al., 2012; Sturm et al., 2001). Liston and Sturm (2002) found that areas of vegetation also impact snow distribution downwind. Wind has a difficult time penetrating vegetation, which causes it to either slow or subside. Hence, the ability for wind to redistribute snow downwind of vegetated areas is limited (Liston and Sturm, 2002) and these areas experience greater snow accumulations (Sturm et al., 2001). A study by Morse et al. (2012) in the outer Mackenzie Delta of Canada found alluvial areas to have greater snow depths than upland areas because the vegetation within alluvial environments trapped snow and prevented it from reaching the uplands. Greater snow depths were also found in areas near water bodies such as rivers and lakes, which are sources of blowing snow (Morse et al., 2012).

Vegetation in both taiga and tundra environments also prevents snow from being sublimated (Liston and Sturm et al., 2002; Sturm et al., 2001). Sublimation increases with high air temperature, low relative humidity, and high wind speeds. Vegetation blocks the wind and restricts high wind speeds from sublimating the snow (Sturm et al., 2001; Liston and Sturm, 2002). However, sometimes the snow is caught in the tree or shrub canopy and does not reach the soil-surface. This snow is not protected and eventually is sublimated back into the atmosphere or melts and falls onto the soil-surface (Callaghan et al., 2011b).

Topography also impacts snow accumulation trends (French, 2007; Liston and Sturm; 2002; Morse et al., 2012). French (2007) made the observation that snow accumulation is greatest on the north side of slopes in the northern hemisphere where there is a decreased amount of solar insolation. The south side of mountains blocks the incoming solar rays and hence, the northern side of slopes experience colder temperatures and less snowmelt (French, 2007). Snow accumulation is also favored in the depressed landscape of valleys and topographic depressions rather than mountain ridges because of decreased radiation and reduced winds (French, 2007; Liston and Sturm, 2002). On the contrary, snow accumulation was less in coastal areas because of higher winds associated with the flat coastal landscape (Liston and Sturm, 2002).

V.2.4 Current Techniques used to Monitor Snow-Cover Characteristics

Snow observations are difficult to obtain because of large spatial variability of snow cover over short distances. Advances have been made in remote sensing to monitor snow cover, and this technique has proven to be a successful and easy method for measuring snow-cover extent. However, snow depth is highly variable and there has been limited success utilizing remote sensing to determine snow thickness. Thus, while remote sensing has successfully measured snow extent, snow depth observations rely primarily upon ground-based measurements.

Studies by Hall et al. (2002), and Dozier and Painter (2004) measured snow extent by using the Moderate Resolution Imaging Spectroradiometer (MODIS) on board the Terra satellite to create snow maps. Dozier and Painter (2004) discussed how the reflectance values of MODIS bands 1 and 6 could be used to calculate the Normalized

Difference Snow Index (NDSI), which designates each pixel in the image as either snow-covered or not snow-covered. This algorithm allows for the creation of snow maps yet variability exists within each pixel and can cause MODIS to overestimate or underestimate snow-cover extent. The study also found it difficult to determine if snow was on the ground when the soil-surface was blocked by vegetation (Dozier and Painter, 2004). MODIS was also used in a study by Hall et al. (2002), which created 8-day imagery composites of MODIS to account for days with unusable imagery caused by cloud cover. The infrared bands of MODIS have thermal properties that can depict ground-surface temperatures, and a pixel would not be mapped as snow-covered if it exceeded 277 K. This method eliminated inaccurate representations of snow caused by cloud cover, aerosol effects, and the confusion of sand as snow.

Some research projects have experimented with remote sensors to make snow-depth observations however, the relatively thin nature and variability of snow is not easy to monitor. Previous studies have used radar to measure snow depth on the North Slope of Alaska (Holmgren et al., 1998). By comparing the frequencies of radar being reflected from both the snow and soil-surface, it was possible to take the frequency difference and determine snow depth. This technique provided faster measurements than would be obtained by snow probing, yet it contained a higher degree of uncertainty. For instance, sometimes a layer of ice within the snow could be mistaken for the ground and cause the radar to be reflected too soon (Holmgren et al., 1998). LIDAR is a relatively new technique that has also been used to collect snow-depth measurements (Sturm et al., 2010). A plane takes LIDAR measurements by flying over the same area before and after the snow accumulates. These measurements allow for snow-depth maps, but can get

expensive by requiring frequent flights over the region where snow-depth measurements are being made (Sturm et al., 2010).

The most effective and inexpensive ways to observe snow depth utilize ground-based techniques. Previous studies have made snow depth observations from the ground using digital cameras, snow probes, gauges, and iButtons, (Laffley et al., 2012; Liston and Sturm, 2002; Lewkowicz, 2008). Laffley et al. (2012) used digital cameras to measure snow cover in a small glacial basin. The cameras provided high spatial and high temporal resolution by taking 3 images daily. The study ran into challenges because the cameras were unsuccessful at acquiring usable night images, and they were sometimes limited by water condensation affecting the lens and other weather conditions. The images produced by the cameras were also at an angle and had to be processed before judgments of snow cover could be made, and the camera batteries had to be replaced frequently (Laffley et al., 2012). Other studies have used snow gauges to measure snow depth, but these are often overestimates because the gauges capture snow which is then not subject to wind redistribution and sublimation (Liston and Sturm, 2002).

In 2008, Lewkowicz made estimates of snow depth using temperature dataloggers. The study placed loggers at 5, 10, 20, 30, 40, 50, 60, 80, and 100 cm above the ground surface and recorded temperature every four hours. Loggers were spaced closer together near the ground because of the non-linear relationship between snow depth and its insulation influences on ground temperatures. The predicted duration for each Thermochron® iButton[2] was more than 8 years. Dataloggers are a low-cost technique for making temperature measurements and they are suitable for areas of permafrost because they can withstand large temperature ranges. When the iButtons

[2] Produced by Maxim Integrated™, San Jose, CA.

began to record temperatures greater than 1 or 1.5°C between adjacent iButtons, the lower iButton was considered snow-covered (Lewkowicz, 2008).

Overall, ground-based techniques are the most effective for measuring snow depth, but these techniques are limited because they rely on data gathered at specific point locations. This study investigated several ground-based techniques to make snow-cover measurements at a series of sites across the Kuparuk region, which vary in both topography and vegetation. An inexpensive technique to measure snow cover over large spatial extents is highly valued by scientists.

V.3 Methodology

V.3.1 Data Availability

CALM air and soil-surface temperature data were utilized in this chapter to estimate SCD between 1996 and 2013. Data availability and collection of CALM temperature data were described in Chapter IV. The location of the CALM study sites are shown in Figure IV-1.

Thermochron iButton® miniature dataloggers were installed at seven of the CALM study sites (U7b, U31, U32a, U32b, U10, U11b and U11c) in 2010 to monitor snow depth. The loggers were affixed to the previously established mast in a vertical array at varying heights (0, 5, 10, 20, 30, 50, 75, and 100 cm), and collected temperature at 4-hour intervals. Researchers visited the sites with iButtons in summer 2011, 2012, and 2013, to maintain the sites and download the data.

In August 2012, Wingscapes®[3] Timelapse Cam cameras were installed to observe snow depth at six CALM sites (U31, U32a, U32b, U10, U11b, and U11c). These cameras have weather-resistant outer cases and were set up to take a digital photograph daily at noon. Data from the 2013 hydrologic year were downloaded in August 2013.

The US Department of Agriculture's (USDA) Natural Resources Conservation Service operates and maintains SNOTEL sites, which collect snowpack and related climatic data in the western United States. SNOTEL has sites at Imnavait, Sagwon, and Prudhoe Bay. These sites have been reporting precipitation data since 1981, 1983 and 2003, respectively using storage precipitation gages. Snow-depth data has also been collected since 2011 at these SNOTEL sites using a sonic sensor (Natural Resources Conservation Service). Since CALM does not collect data on precipitation and was just beginning to test new methods for gathering snow-depth data, this chapter analysis utilizes the snow depth and precipitation data gathered by SNOTEL. The Prudhoe Bay SNOTEL site is located in subzone C, but was still included in this analysis because precipitation and snow depth measurements are so rare in the study area. Data from Prudhoe Bay was utilized to represent subzone D. Figure V-1 displays SNOTEL sites, and sites instrumented with iButtons and with time-lapse cameras.

[3] Purchased from EBSCO Industries.

Figure V-1 Map showing the locations of SNOTEL sites and CALM study sites instrumented with iButtons and cameras, in the Kuparuk region. Bioclimatic subzones and the physiographic boundary are shown.

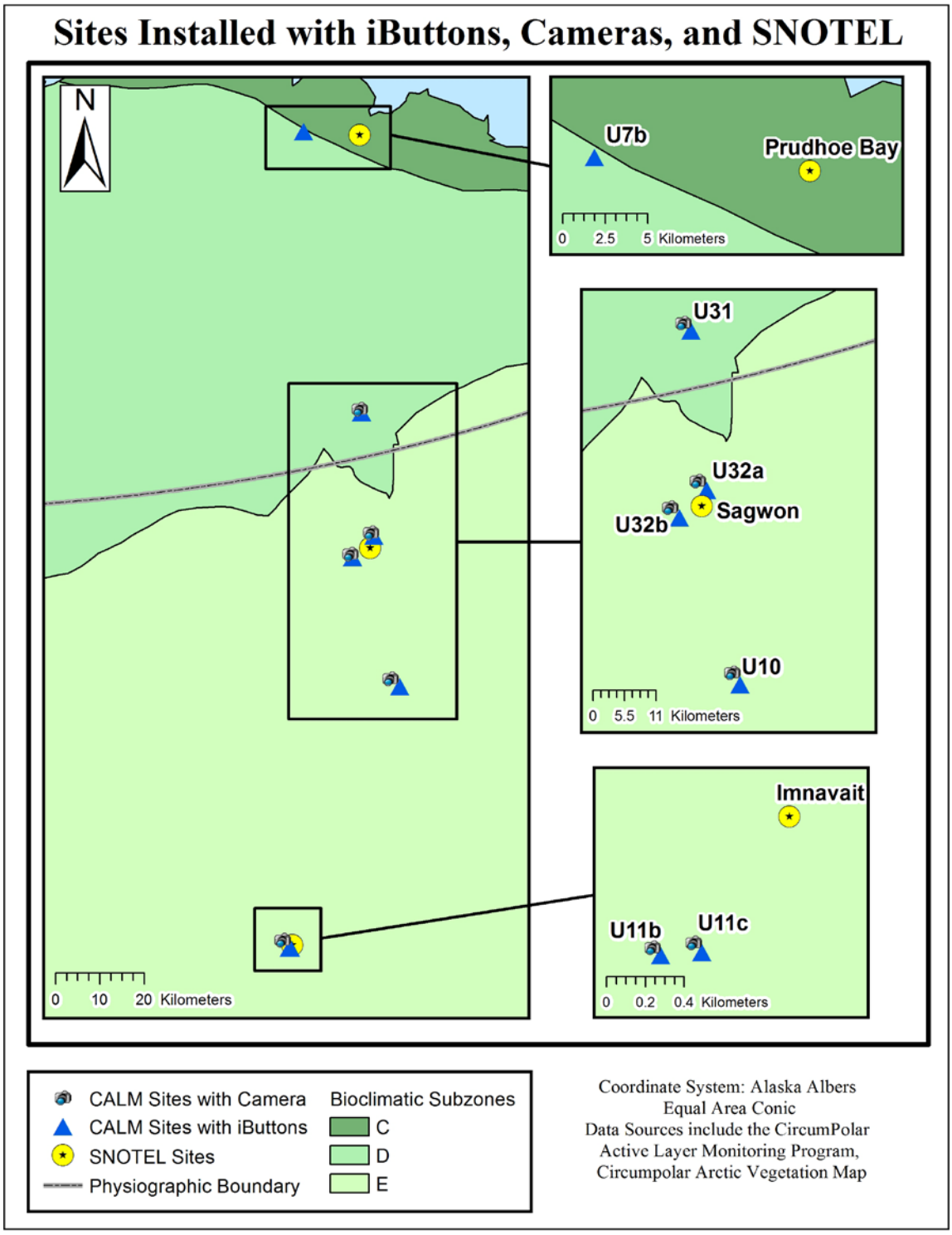

V.3.2. Data Analysis

Both the daily soil-surface temperature amplitude and the mean daily air temperature data collected by the CALM program were used to interpret SCD for each hydrologic year at each site. Snow acts as a buffer and retains heat in the underlying ground that it covers during the winter. Therefore, soil-surface temperatures are expected to be warmer than winter air temperatures when the ground is snow-covered (Morse et al., 2012). Snow also keeps the underlying ground at a nearly constant temperature, so the soil-surface amplitude should be small for snow-covered ground (Decker, 2003). Days at each site were considered snow-covered if they experienced a mean daily air temperature of less than 0 °C and daily soil-surface temperature amplitude of less than 1°C. At first, the date of snow onset was determined as being the first day upon which snow-covered days remained continuous, however this method was inaccurate because sometimes there would be a set of several snow-covered days followed by a set of snow-free days. Thus, rules for determining the date of snow onset and snowmelt were derived. The date of snow onset was obtained by finding the day of a consecutive set of 5 snow-covered days within the months August to November unless 10 consecutive snow-free days followed. Similarly, the date of snowmelt was obtained by finding the first day of the year when snow-free days became consistent in the spring, utilizing 5 and 10 day thresholds of snow-free and snow-covered observations. SCD was the count of days between the dates of snow onset and snowmelt. The SCD measurements were aggregated into subzones by averaging yearly SCD measurements made at each site between all sites in the subzone (subzone D = U7b, U7c and U31; subzone E = U32a, U32b, U12b, U11b, U11c and U10).

Periods between the date of snow onset and snowmelt, when air temperatures exceeded 0 °C and soil-surface temperature amplitudes remained less than 1 °C, were considered as freeze/thaw cycles affecting the upper portion of the snowpack. A small soil-surface amplitude indicated that the ground was still snow-covered and higher air temperatures were assumed to thaw the top of the snowpack. The thawed snow was considered to re-freeze once temperatures fell below 0 °C again and hence, this event was identified as a freeze/thaw cycle. One freeze/thaw cycle lasts from the first day the conditions exist until the day on which air temperatures fall below 0 °C again. The mean yearly number of freeze thaw cycles was determined for both subzones D and E.

Following Lewkowicz (2008), iButtons were utilized to interpolate snow depth at CALM sites with data available. Lewkowicz considered iButtons to be snow-covered when adjacent loggers recorded mean daily temperature differences greater than 1 or 1.5 °C. In this study, the iButton datasets were compiled and processed into mean daily temperatures, aggregated by bioclimatic subzone, and examined by hydrologic year. When the temperature difference between adjacent iButtons in the vertical array was greater than or equal to 1°C, the lower logger was considered to be snow-covered. Measurements of snow depth were estimated as halfway between the lower snow-covered logger and the adjacent snow-free upper logger.

There was a very low success rate of the iButtons in this research, which promoted the installation of time-lapse cameras to attempt to monitor snow depth. Three stakes were positioned in front of each time-lapse camera with markings every five centimeters, ranging from zero to one hundred. The three stakes were positioned at a range of local micro-topographic heights; lowest, middle and highest. Figure V-2 shows

the masts at the six sites installed with time-lapse cameras. A visual analysis of the images was used to measure the daily snow depth at each site for the 2013 hydrologic year. The daily mean snow depth at each site was calculated as the mean of the three stakes.

Figure V-2 Three stakes situated at different micro-topographic heights in front of the time-lapse camera at sites U32a (a), U32b (b), U11b (c), U11c (d), U10 (e) and U31 (f).

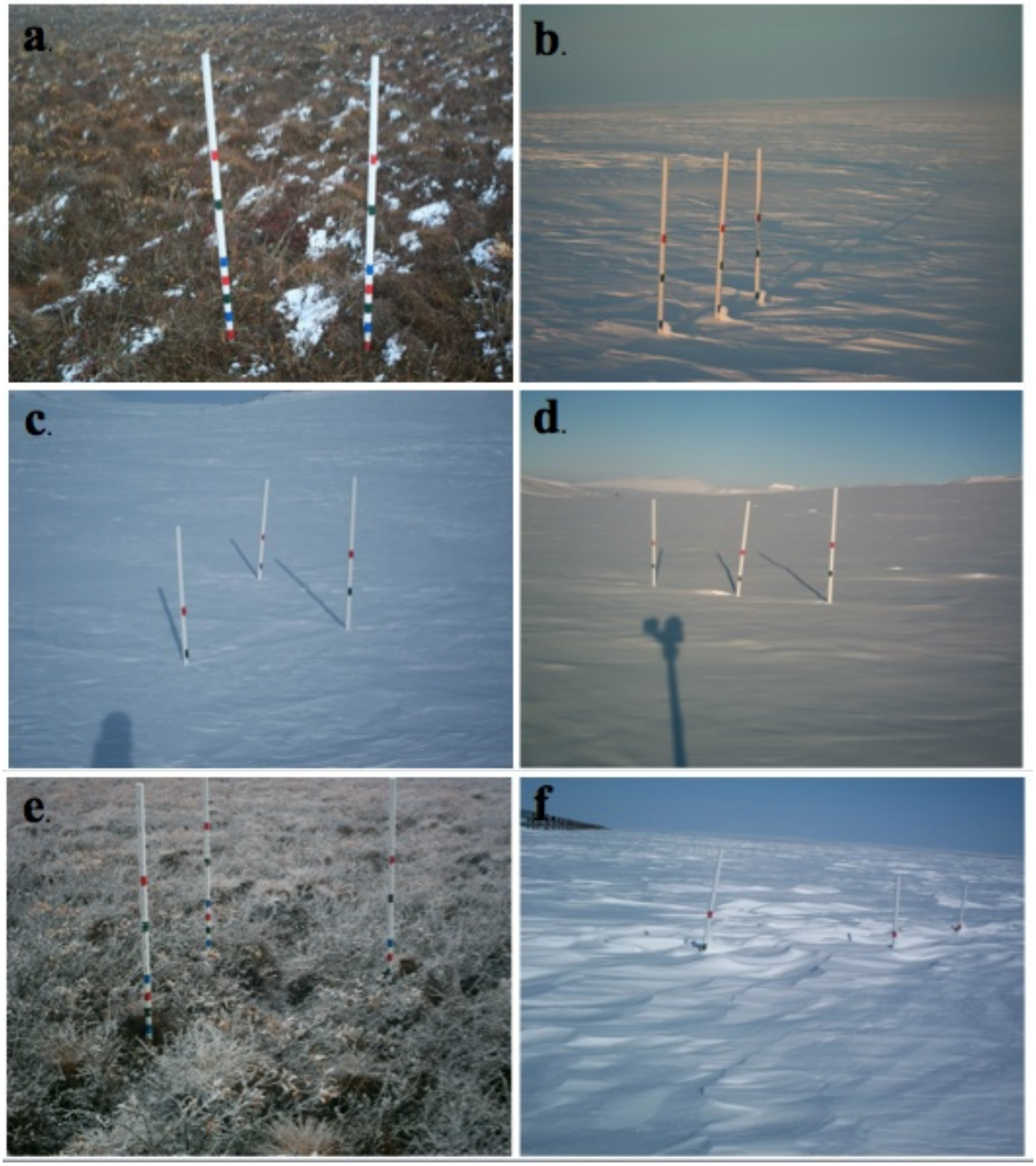

Previous studies have used precipitation accumulation collected by SNOTEL to estimate snow depth by summing the precipitation from October to May, yet this method did not account for snow flowing or drifting (Klene et al., 2008). This study utilizes a linear regression analysis between SNOTEL's snow-depth and accumulated-precipitation data collected during the 2012 and 2013 hydrologic years to produce linear regression equations for Prudhoe Bay, Sagwon, and Imnavait. These regression equations were used to estimate snow depth at SNOTEL sites from 2005 to 2013 when precipitation data were available but not snow observations.

SNOTEL annual accumulated precipitation data began at 0 cm on September 1 and was measured until August 31 each year. This allowed for the total accumulated precipitation to be measured for each hydrologic year. Precipitation data did not start being collected at Prudhoe Bay until the middle of the 2004 hydrologic year and thus, precipitation measurements for subzone D were only available for the 2005 hydrologic year onward.

For the linear regression equations, all available snow depth data from SNOTEL was used. Sometimes more than one snow-depth measurement occurred for each precipitation value. For instance, when the accumulated precipitation in 2013 was 9.9 cm at Sagwon from January 9- 12, snow depth values were 40.6 cm on January 9 and 33.0 cm on January 10- 12. These multiple snow depth values were averaged together to obtain the mean snow depth that occurred when accumulated precipitation was 9.9 cm that year. Doing this created a more linear trend in the relationships between snow depth and precipitation at each site.

The accumulated precipitation data at each SNOTEL site was then used in the equation to estimate snow depth at Prudhoe Bay, Sagwon, and Imnavait. Only years with a full set of precipitation data were able to have their snow depth estimated because otherwise total accumulated precipitation values were unable to be obtained.

V.4 Results

V.4.1 Snow-Cover Duration from Air and Soil-Surface Temperatures

The mean SCD was 247 days in subzone D with a decreasing trend of 0.6 days per year (Figure V-3). Maximum values of SCD decreased 0.7 days per year and minimum values decreased 0.8 days per year. Single points on the graph represent years when only two or less sites in the subzone had SCD measurements made, and these points were not used to calculate the trend. Site U31 was unable to provide SCD estimates for hydrologic years 1996, 2005, 2009 and 2011, because of missing soil-surface temperature data. Similarly, site U7c was unable to have SCD calculated in 1997 and 2011 because of a lack of soil-surface temperature data.

Figure V-3 The maximum, mean, and minimum SCD in subzone E between 1996 and 2013 estimated from air and soil-surface temperatures. Single points on the graph not associated with the trendline represent years when only two or fewer sites in the subzone had SCD data available.

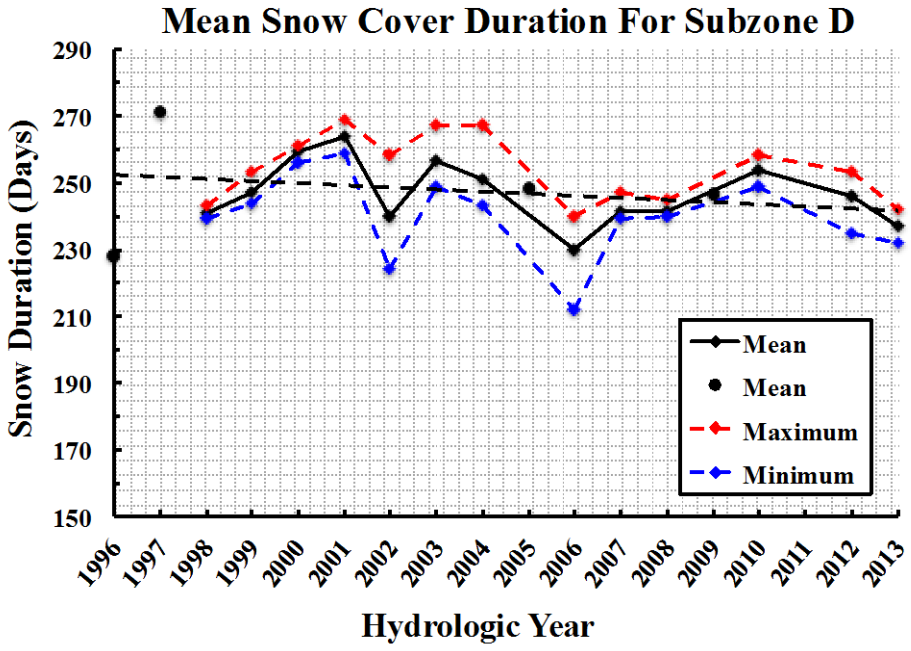

Figure V-4 shows that the mean date of snow onset in subzone D is becoming slightly later (0.6 days per year). The mean date of snow onset for the study period was September 23, and the earliest mean date of snow onset was estimated to be September 7 in 1997. The latest mean date of snow onset in 2006 is attributable to the later snow onset (October 23) at site U7b. The maximum, mean, and minimum dates of snow onset in 2003 were very similar because the dates of snow onset at all sites in subzone D were within one day. The mean date of snow onset during the study period at sites U7b and U7c was September 24, while the mean date of snow onset at site U31 was September 20. Thus, site U31 experienced the earliest dates of snow onset in subzone D.

Figure V-4 Maximum, mean, and minimum dates of snow onset estimated in subzone D between 1996 and 2013. Years when two or fewer study sites were able to have snow onset determined are represented as single points and were not utilized to calculate the trend.

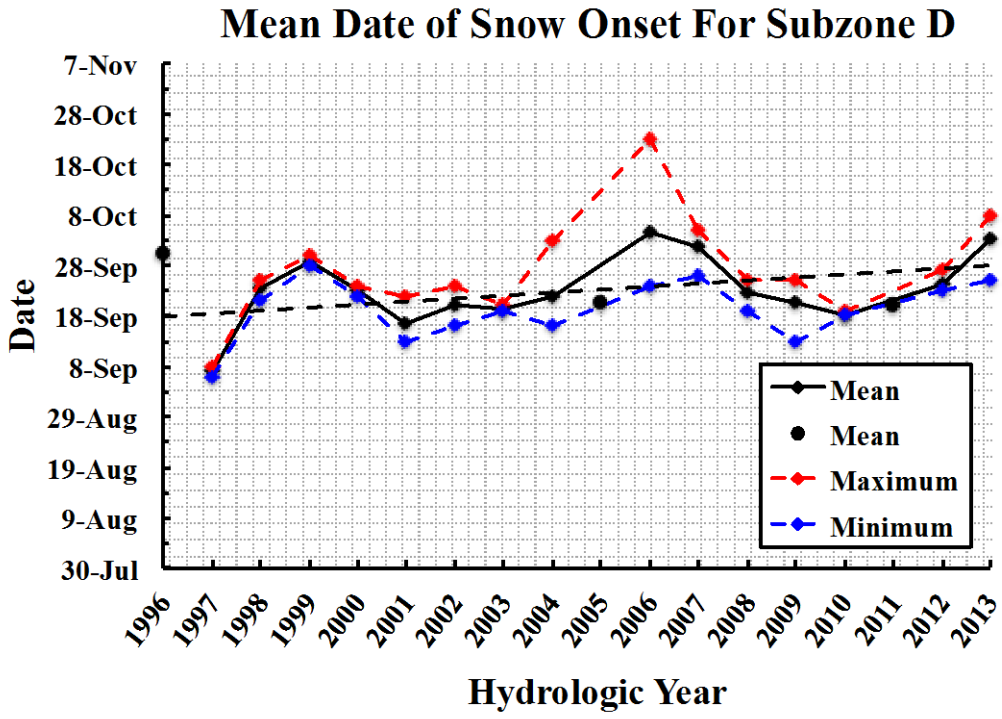

The mean date of snowmelt in subzone D came earlier by 0.2 days per year over the study period (Figure V-5). The mean date of snowmelt was May 29. Minimum and maximum values for the date of snowmelt came earlier by 0.3 days and 0.2 days respectively, per year. During 2006, 2007, and 2008, the maximum, mean, and minimum estimated dates of snowmelt were similar because all study sites in subzone D had snowmelt within one day. The latest date of snowmelt was estimated to be June 15 at site U7c in 2003.

Figure V-5 Maximum, mean, and minimum dates of snowmelt estimated in subzone D between 1996 and 2013. Years when two or fewer CALM study sites were able to have the date of snowmelt determined are represented as single points on the graph and were not utilized to calculate the trend.

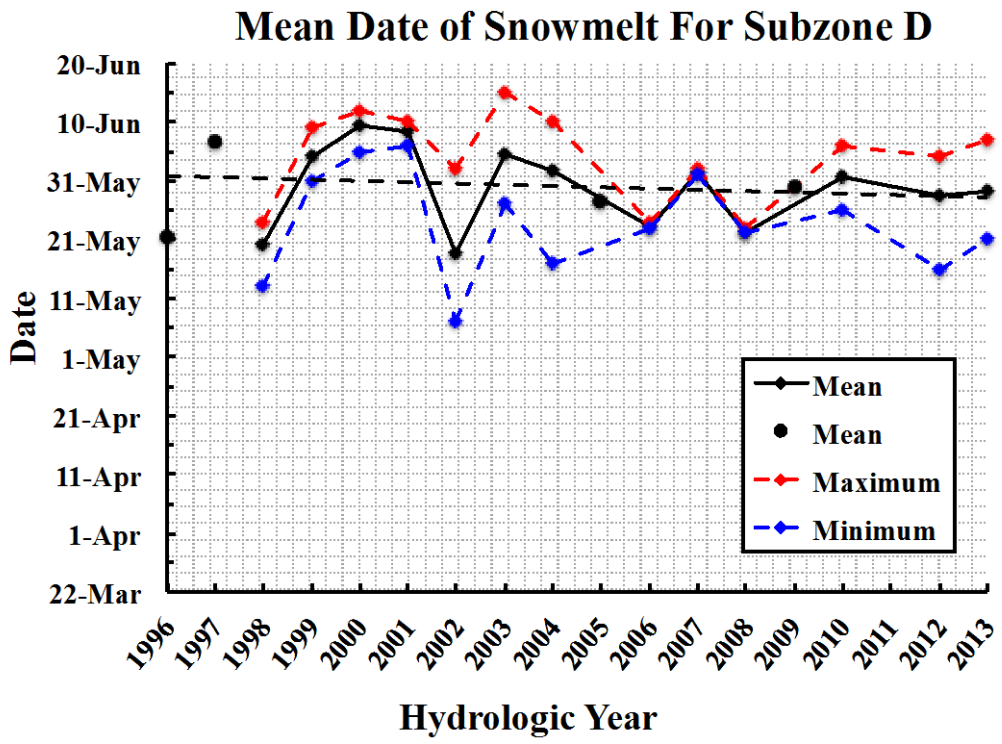

SCD in subzone E was on average 238 days and increased 0.4 days per year (Figure V-6). The low SCD in 1996 was because of low SCD estimates at sites U12b, U11b, U11c, and U10, which were all below 200 days. If the 1996 hydrologic year were emitted from this analysis, SCD would show a decreasing trend of 0.4 days per year in subzone E. A late date of snow onset was experienced in 1996 (U12b, U10, and U11c), when 5 consecutive snow-covered days did not occur till late October or November. Two sites also had very early dates of snowmelt in April during the 1996 hydrologic year (U11b and U11c). Up to 9 consecutive snow-covered days occurred in mid-May at some sites but 10 snow-covered days were needed to occur after 5 consecutive snow-free days in order for the earlier date to not be considered the date of snowmelt. Finally, the maximum, mean, and minimum SCD were equal in 2011 because all sites in subzone E had a SCD of 238 days. Overall, estimates of SCD were longer in subzone D than E by an average of 9 days. Soil-surface temperatures were colder in subzone D than subzone E, indicating that SCD may not be a major determinant of soil-surface temperatures if it is a thin snow cover.

Figure V-6 Maximum, mean, and minimum SCD estimated in subzone E between 1996 and 2013.

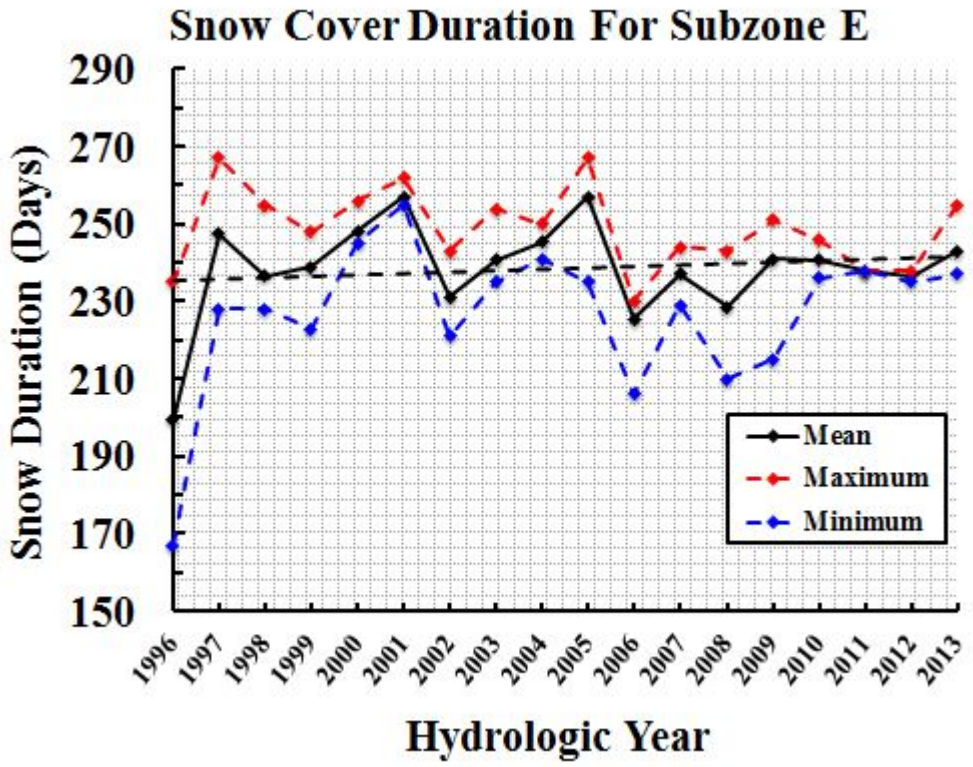

The mean date of snow onset in subzone E was September 21 and came earlier by 0.28 days per year (Figure V-7). The maximum and mean dates of snow onset were later in the year during 1996 at CALM sites U12b, U10 and U11c, and were discussed earlier. Two other late dates of snow onset occurred in 2006 (Oct 18) and 2008 (Oct 15). In 1997, 2000, 2004, and 2010, all sites had a date of snow onset within 2 days of each other and in 2011 all sites experienced the same data of snow onset (Sep 20). Overall, the dates of snow onset in both subzones were relatively similar with the mean date of snow onset 2 days later in subzone D.

Figure V-7 Maximum, mean, and minimum dates of snow onset estimated in subzone E between 1996 and 2013.

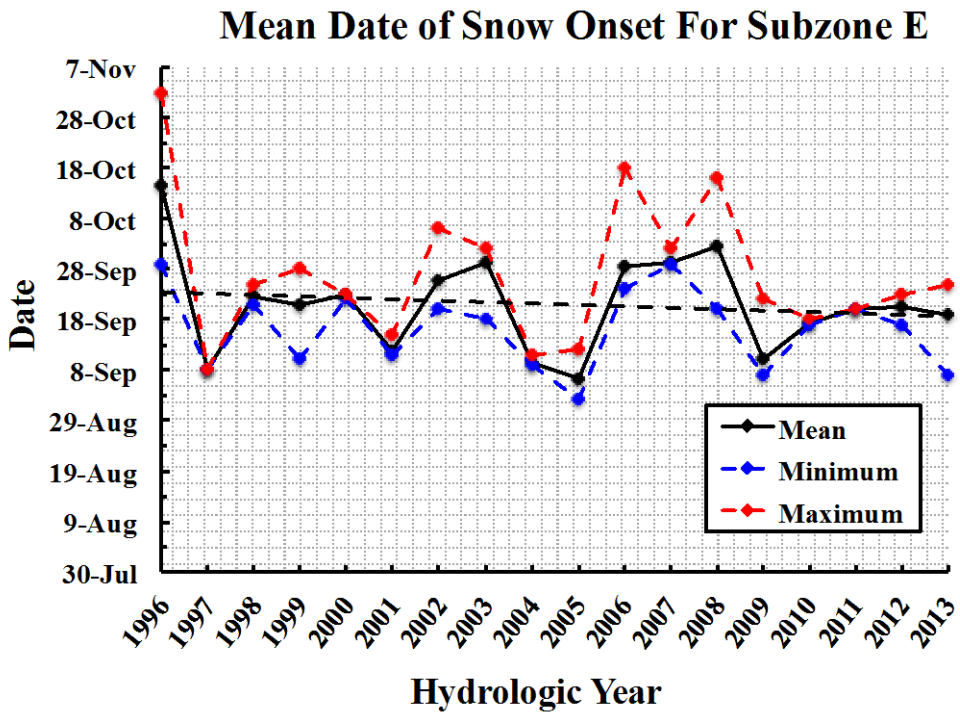

The mean date of snowmelt in subzone E during the study period was May 17 and came later by 0.21 days per year (Figure V-8). The early (minimum) and mean date of snowmelt in 1996 are attributable to the early snowmelt at sites U11b and U11c, which both experienced snowmelt on April 17. The earliest dates of snowmelt were in 2005 and 2009, where the snowmelt occurred on April 26. In 2011, all sites that had data to estimate SCD in subzone E experienced snowmelt on May 17. In 2012, the date of snowmelt at all sites was either May 15 or 16. Overall, subzone E experienced earlier dates of snowmelt than subzone D by about 12 days each year.

Figure V-8 Maximum, mean, and minimum dates of snowmelt estimated in subzone E between 1996 and 2013.

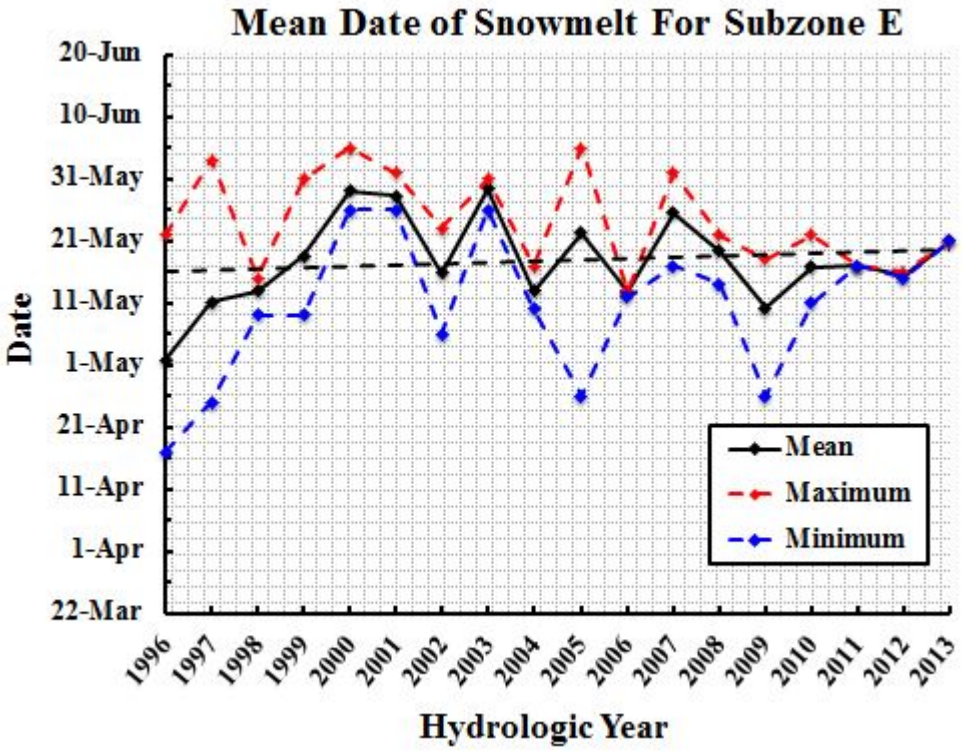

Freeze/thaw cycles decreased slightly in subzone D (0.0 days per year) and remained steady in subzone E (Figure V-9). The annual mean number of freeze/thaw cycles for the study period was 2 in subzone D, and 3 in subzone E. Only years that had sufficient data available to estimate SCD could be used to estimate the number of freeze/thaw cycles and thus, subzone D was unable to have freeze/thaw cycles calculated in 2011. Subzones D and E experienced the highest number of freeze/thaw cycles in 2004. The higher number in subzone E may be attributable to slightly warmer winter air temperatures. This factor may enhance the frequency of rain-on-snow events, which are tied to the frequency of freeze/thaw cycles. The shorter SCD in subzone E compared to D may be partly attributable to the greater number of freeze/thaw cycles there.

Figure V-9 Annual number of freeze/thaw cycles estimated in subzones D and E between 1996 and 2013.

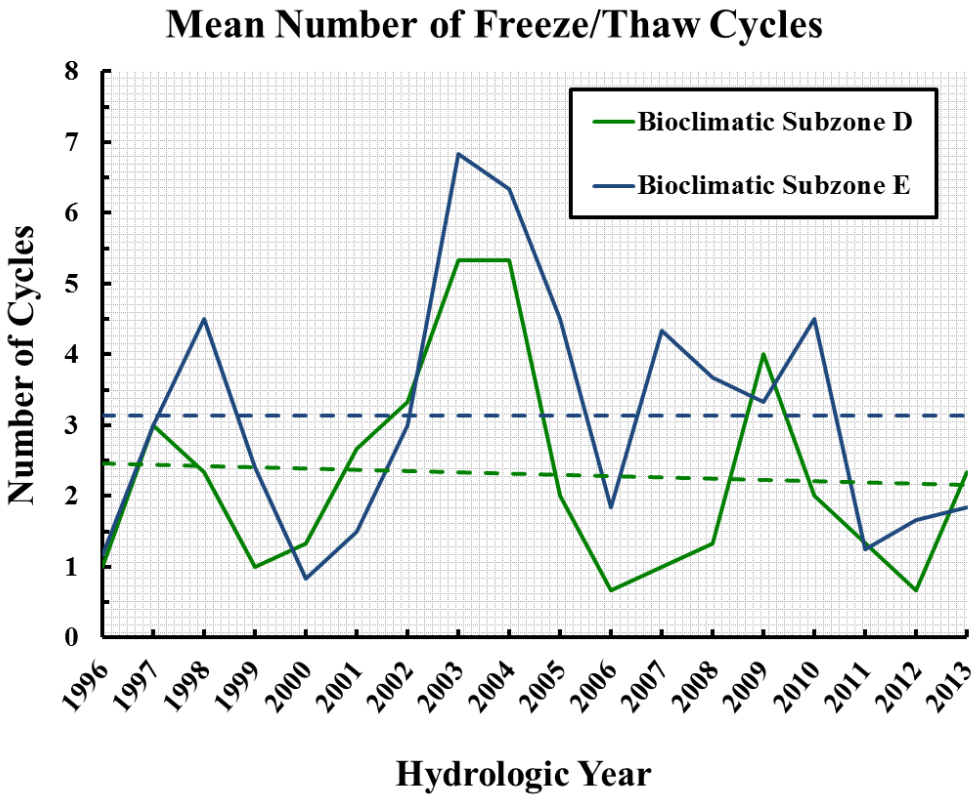

V.4.2 SCD and Snow Depth from Vertical Arrays of Temperature Dataloggers.

According to Table V-1, only one site had a complete data record from all eight iButtons in an array for one year and this was site U11b in 2012. In 2011, four of the six sites with iButton arrays had a success rate of 50% or lower. In 2012, four of the seven sites with iButton arrays had a success rate of 50% or lower, and three of these sites had no records recovered at all. The overall success rate of the iButtons in this study was 48 %. This success rate is lower than in other previous studies. Lewkowicz (2008) reported an 80 % success rate using iButton's to measure snow depth. It is possible that the tape used to affix the iButton's to the stakes in this study may have caused moisture to become trapped and for the iButtons to be inoperative, or weather conditions may have also been a factor. Although iButtons are water resistant, they are not waterproof. Animals did chew on the tape used to attach the loggers but in almost all the cases the loggers were recovered from near the base of the stake and none appeared damage.

Table V-1 Table showing CALM sites where iButtons were installed (N.A. means no iButtons installed). The number of iButtons in the array from which data were successfully retrieved at each site is shown.

Successful iButtons		
Site	**2011**	**2012**
U7b	N.A.	0
U7c	N.A.	N.A.
U31	5	0
U32a	4	4
U32b	4	6
U12b	N.A.	N.A.
U11b	4	8
U11c	4	5
U10	6	0

The data retrieved from the array of iButtons at site U11b in subzone E showed that snow depth increased gradually during the early winter (Figure V-10). The greatest snow depths were reached during February, March, and April, and a rapid period of snowmelt followed in late May. The dates of snow onset and snowmelt were 25 September 2011 and 24 May 2012, with a SCD of 242 days. The abrupt changes in snow depths during the winter months may be attributable to wind redistribution. The graphs show such large changes in snow depth during the winter because as snow depth increases, the interval between adjacent iButtons increases. For example, when the iButton at 75 cm was snow-covered, snow depth was recorded to be 87.5 (halfway between the 100 cm iButton and 75 cm iButton). If the adjacent iButton at 50 cm was the highest snow-covered iButton, snow depth was recorded as 62.5 cm.

The estimate of SCD made using the air and soil-surface dataloggers at site U11b during the 2012 hydrologic year was 238 days, with snow onset on 19 September and snowmelt on 15 May. Overall, both datalogger techniques provided similar results for SCD, but the dates of snow onset and snowmelt differed by about a week, with the air and soil-surface temperatures occurring earlier in each case.

Figure V-10 Snow-pack development at site U11b in subzone E. Snow depths were interpolated from mean daily temperatures recorded by the vertical array of iButtons.

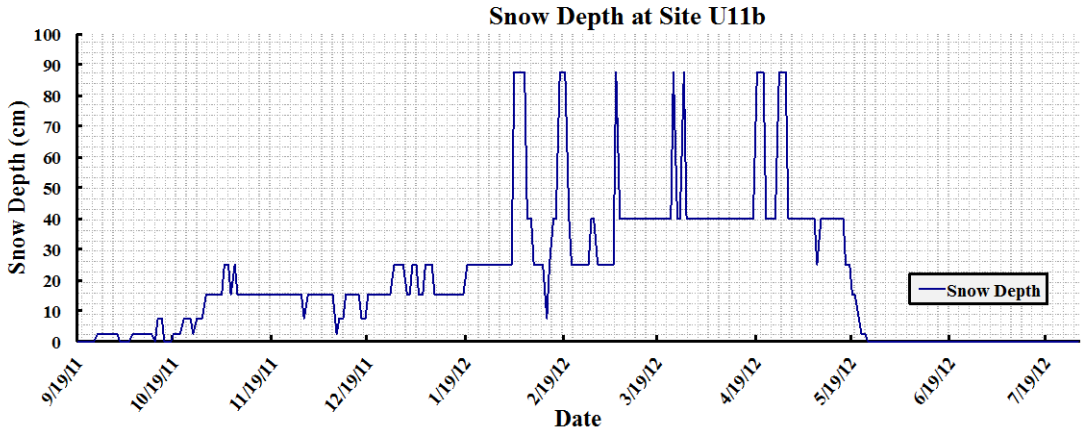

The temperatures from the iButton array at site U11b during the snow onset and snowmelt periods are shown in Figure V-11. During snow onset, iButtons closest to the ground became snow-covered and displayed mean temperature readings greater than those displayed by iButtons exposed to ambient air temperatures (Figure V-11a). The iButton located at 0 cm became snow-covered first on September 25, as indicated in Figure V-12a and the temperature difference between the 0 cm iButton and the rest of the iButtons. In November the 0, 5, and 10 cm iButtons were all snow-covered and displayed warmer temperatures than the rest of the higher iButtons. The warmer temperatures of the snow-covered iButtons are attributable to the insulation provided by the snow cover and the slow transfer of cold temperatures into the snowpack. The snow-covered iButtons closer to the ground also have the warmest temperatures because they are adjacent to the ground.

In contrast, iButtons exposed to ambient air temperatures during the snowmelt period become warmer than those still snow-covered (Figure V-11b). Around May 9, all

iButtons had the same temperature as air temperatures rose and became as warm as the temperatures within the snowpack. After this date iButtons within the snowpack became colder than iButtons exposed to ambient air temperatures. The 0 cm iButton had the coldest temperatures out of all the iButtons in the array on May 23, the day before the date of snowmelt.

Similar to Lewkowitz (2008), this study found iButtons to be a challenging technique for measuring snow depth, especially during the snowmelt period when temperatures above the snowpack became warmer than temperatures within it. This made it very challenging to decipher the date of snowmelt. The use of this technique for measuring snow accumulation also possibly underestimated snow depth during times of deep snow cover because the iButtons in the vertical array only went up to a height of 100 cm. Also, since a comparison between neighboring iButtons was used to interpret snow depth, 87.5 cm (halfway between 75 and 100 cm) was the maximum inferred snow depth when the 75 cm iButton was interpreted as snow-covered.

Figure V-11 Temperature records from the vertical iButton array showing data utilized to estimate (a) snow onset and (b) snowmelt at site U11b in subzone E.

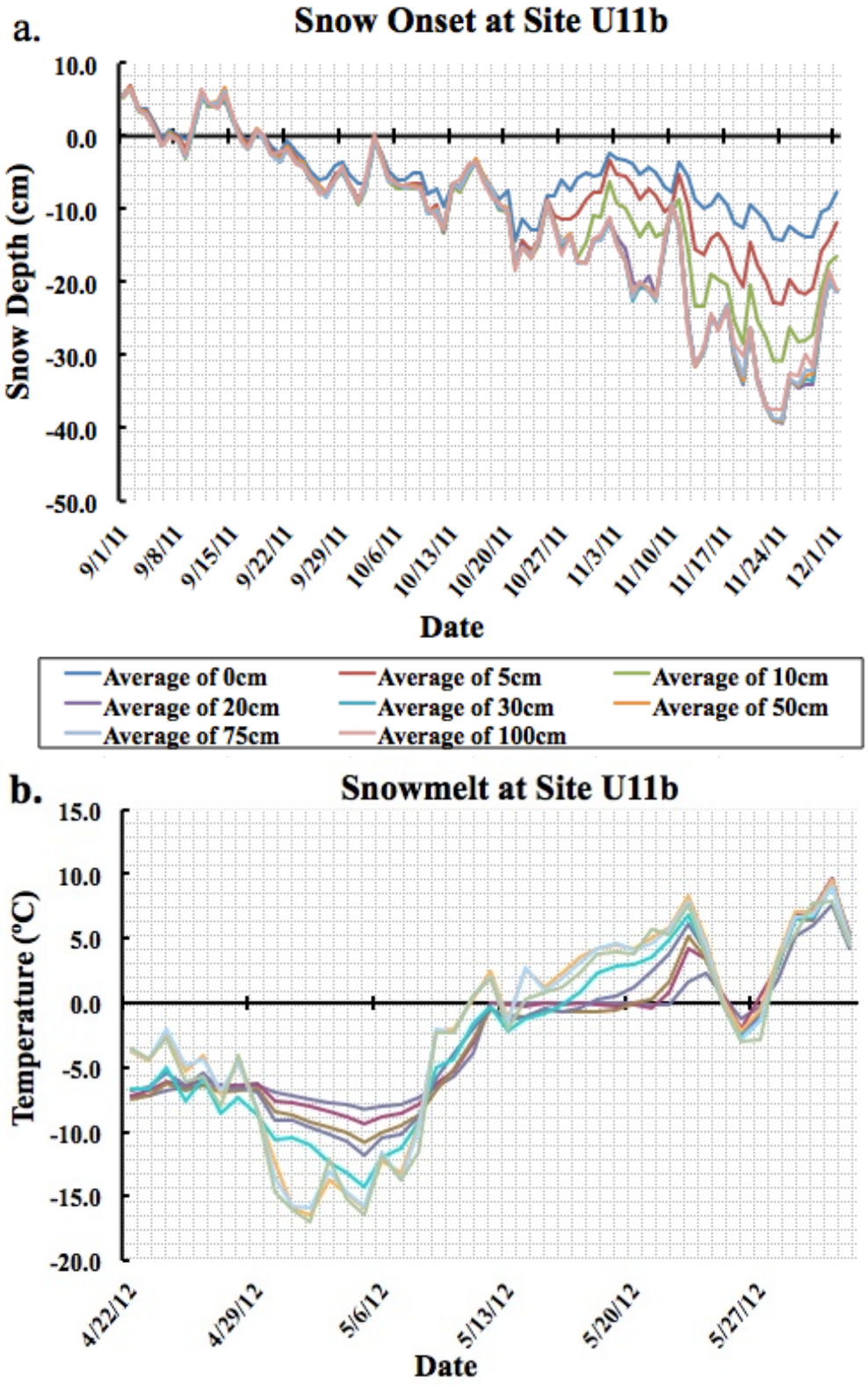

V.4.3 SCD and Snow Depth from Time-lapse Cameras and SNOTEL Data

Of the six time-lapse cameras installed at the study sites, only three were successful at making yearlong measurements of snow depth during their first year of operation. The camera located at site U11c was unable to provide a measurement for SCD because it did not take images in May and June, but automatically resumed taking pictures in July. Two other cameras (U32a, U10) turned down toward the ground in September and were unable to provide snow-depth observations. During the winter it was common for collected images to either be green, completely white, or dark. This resulted in discontinuous daily measurements. However, the cameras at sites U31, U32b, and U11b were able to provide discontinuous snow depth measurements throughout the winter.

Snow depth and duration observations made using time-lapse cameras at sites U31, U32b, and U11b during the 2013 hydrologic year are shown in Figure V-12. Snow-depth observations made using the cameras are shown with large gaps because of the discontinuity of readable images, especially during the winter months. All graphs show differences in snow depth observations between CALM sites and the closest SNOTEL sites, attributable to the large spatial variability of snow cover even over short distances.

Snow depths observed at site U31 are shown in Figure V-12a with SNOTEL precipitation and snow depth data collected at the Prudhoe Bay SNOTEL site. The total precipitation measured at Prudhoe Bay was 165.1 mm for the 2013 hydrologic year. Snow depth observations at site U31 are greater than those at Prudhoe Bay, and this may be caused by wind and differences in microtopography between the sites. The maximum snow depth at the end of April was measured to be 95 cm.

Using the camera at site 31, the dates of snow onset and snowmelt were found to be 8 October 2012 and 10 June 2013. SCD made using the camera was 245 days, while it was calculated to be 237 days using the air and soil-surface temperature dataloggers.

Figure V-12b shows the discontinuous snow-depth observations made using the time-lapse camera at site U32b, along with SNOTEL's snow depth and precipitation observations made at Sagwon. The total precipitation at Sagwon was 172.72 mm for the 2013 hydrologic year, which is very similar to values at Prudhoe Bay. Snow-depth observations made using the camera at site U32b were greater than observations made at the Sagwon SNOTEL. The maximum observed snow depth made using the camera was 72 cm at the end of April, which was thinner than the snow depth observed at site U31 (Figure V-12b).

Using the time-lapse camera, the dates of snow onset and snowmelt were approximately 26 September 2012 and 8 June 2013, with a SCD of 255 days. SCD was estimated to be 237 days using the air and soil-surface temperature dataloggers in 2013. The maximum observed snow depth made using the camera was 72 cm at the end of April, which was thinner than the snow depth observed at site U31 (Figure V-12b).

Snow-depth observations made using the time-lapse camera at site U11b are shown in Figure V-12c, along with precipitation and snow depth observations from the Imnavait SNOTEL. The maximum snow depth at Imnavait was only slightly greater than snow depth observed at site U11b in 2013. The Imnavait SNOTEL and site U11b are located at the top and bottom of a large hill, respectively and thus, differences in snow depth may be attributable to topographic location. Compared to the Prudhoe Bay and Sagwon SNOTEL sites, the total precipitation for the 2013 hydrologic year was slightly

higher at Imnavait and reached 180.34 mm. The maximum snow depth observed at site U11b with the camera at the end of April was 92 cm, which was greater than observations at site U32b but less than at site U31 (Figure V-12c). Overall, snow depth exhibited substantial variability between the CALM and SNOTEL sites.

The dates of snow onset and snowmelt at site U11b were 7 September 2012 and 11 June 2013 using the camera, resulting in a SCD of 277 days. This was almost three weeks longer than SCD measurements made using the air and soil-surface temperature dataloggers (255 days) in 2013.

Figure V-12 Snow depth at sites U31 (a), U32b (b) and U11b (c), observed using time-lapse cameras during the 2013 hydrologic year are shown. SNOTEL precipitation and snow depth data collected at Prudhoe Bay (a), Sagwon (b), and Imnavait (c) are also shown.

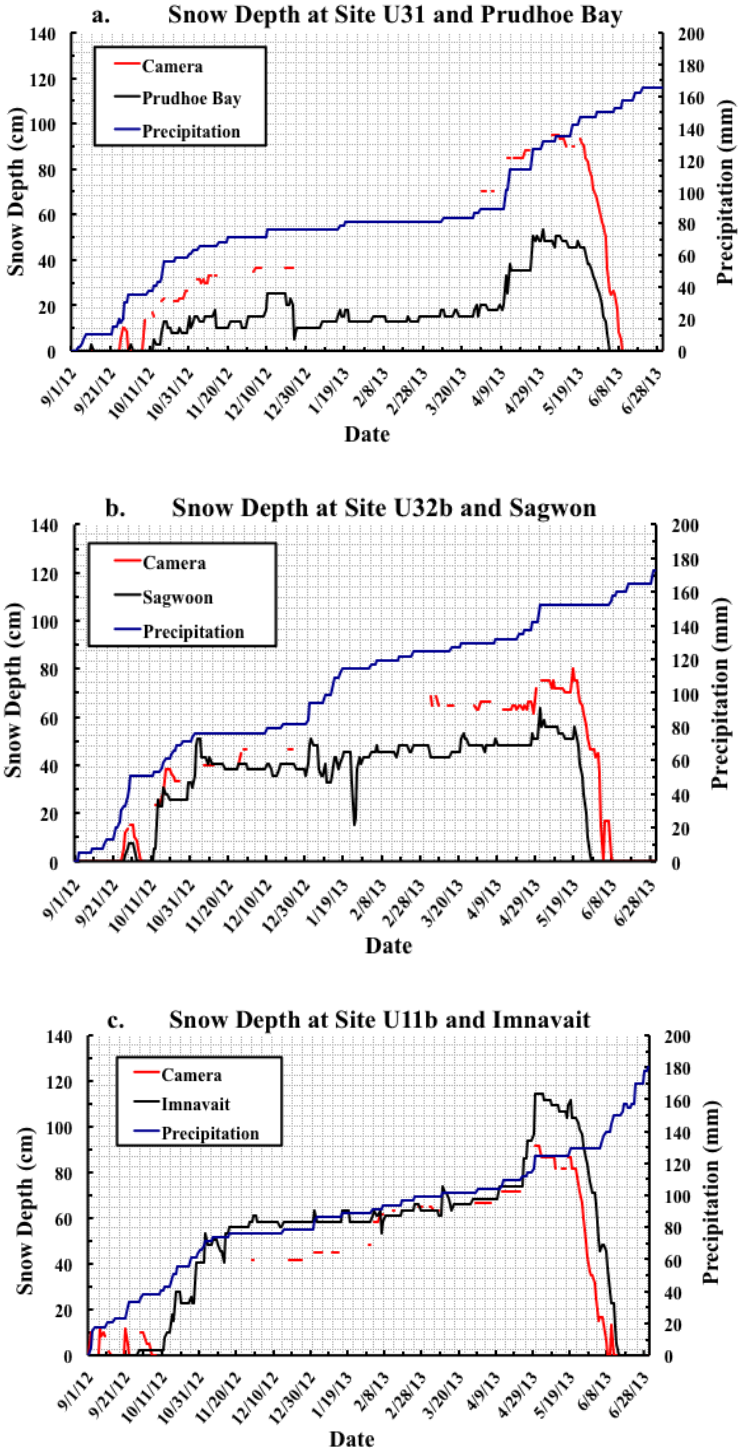

Accumulated precipitation increased at Prudhoe Bay and decreased at the Imnavait and Sagwon SNOTEL sites during the study period (Figure V-13). At Prudhoe Bay, mean annual precipitation was 18.5 cm and this mean increased 0.2 cm per year. Total mean annual precipitation decreased 0.1 cm per year at Sagwon and was 21.6 cm. Similarly, the mean accumulated precipitation decreased at Imnavait by 0.3 cm per year and was 32.5 cm. The maximum annual precipitation observed at Imnavait was in 2000 at 45.5 cm. Overall, accumulated precipitation showed a decreasing trend from south to north in the study area, with the most southern and highest elevation site (Imnavait) having the greatest amount of precipitation.

Figure V-13 Accumulated precipitaiton observed at SNOTEL sites in Prudhoe Bay, Sagwon, and Imnavait between 1996 and 2013.

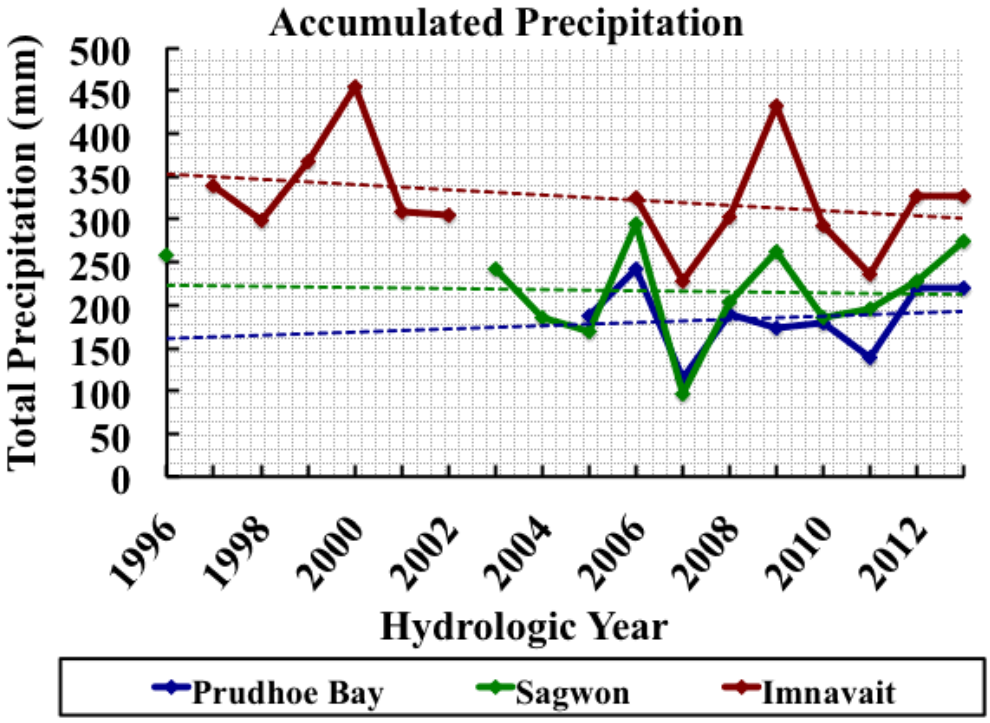

The linear-regression equations derived from SNOTEL snow depth and accumulated precipitation data for the Prudhoe Bay, Sagwon, and Imnavait SNOTEL sites are shown in Figure V-14. These three regressions illustrate how snow depth increases in the foothills. The equations were used to estimate snow depths using SNOTEL precipitation data between the years 2005 to 2013 at Prudhoe Bay, and 1996 to 2013 at Sagwon and Imnavait.

Figure V-14 Relation of SNOTEL snow depth and accumulated precipitation data from the 2012 and 2013 hydrologic years at Prudhoe Bay, Sagwon, and Imnavait.

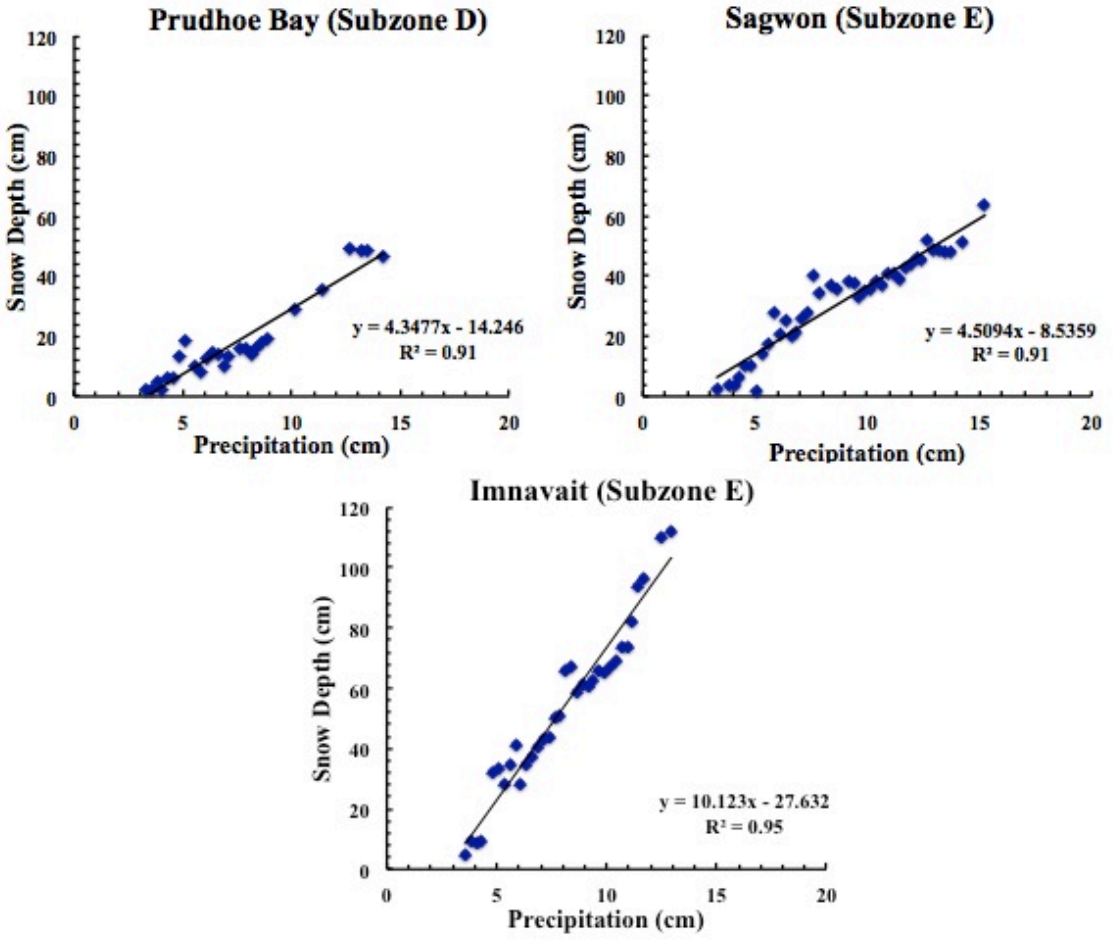

Snow depth was extrapolated for Prudhoe Bay, Sagwon, and Imnavait using the SNOTEL regression equations and accumulated precipitation data (Figure V-15). Prudhoe Bay was only able to have snow depth estimated from 2005 to 2013, while Sagwon and Imnavait were able to have snow depths estimated from 1996 to 2013. Days when minimum snow depth was 0 cm at SNOTEL sites are attributable to accumulated precipitation not being large enough to produce snow depth in the regression equation. Prudhoe Bay had the lowest calculated snow pack with an average mean snow depth of 16.3 cm from 1 November to 30 April (Figure V-15a). The range between maximum and minimum snow depths was 22.11 cm at Prudhoe Bay.

Sagwon had greater snow depths than Prudhoe Bay, with a mean snow depth of 26.4 cm (Figure V-15b). The average daily range between maximum and minimum snow depths was also larger with a mean of 30.8 cm at Sagwon.

Of the three SNOTEL sites, Imnavait had the deepest estimated snow depths and also the greatest range. The mean snow depth at Imnavait was 61.1 cm and the average range was 84.7 cm, almost 4 times the range of Prudhoe Bay (Figure V-15c).

Figure V-15 Mean maximum, mean, and minimum snow-depth progression at Prudhoe Bay (a), Sagwon (b), and Imnavait (c) calculated using SNOTEL accumulated precipitation and the regression equations from each SNOTEL site.

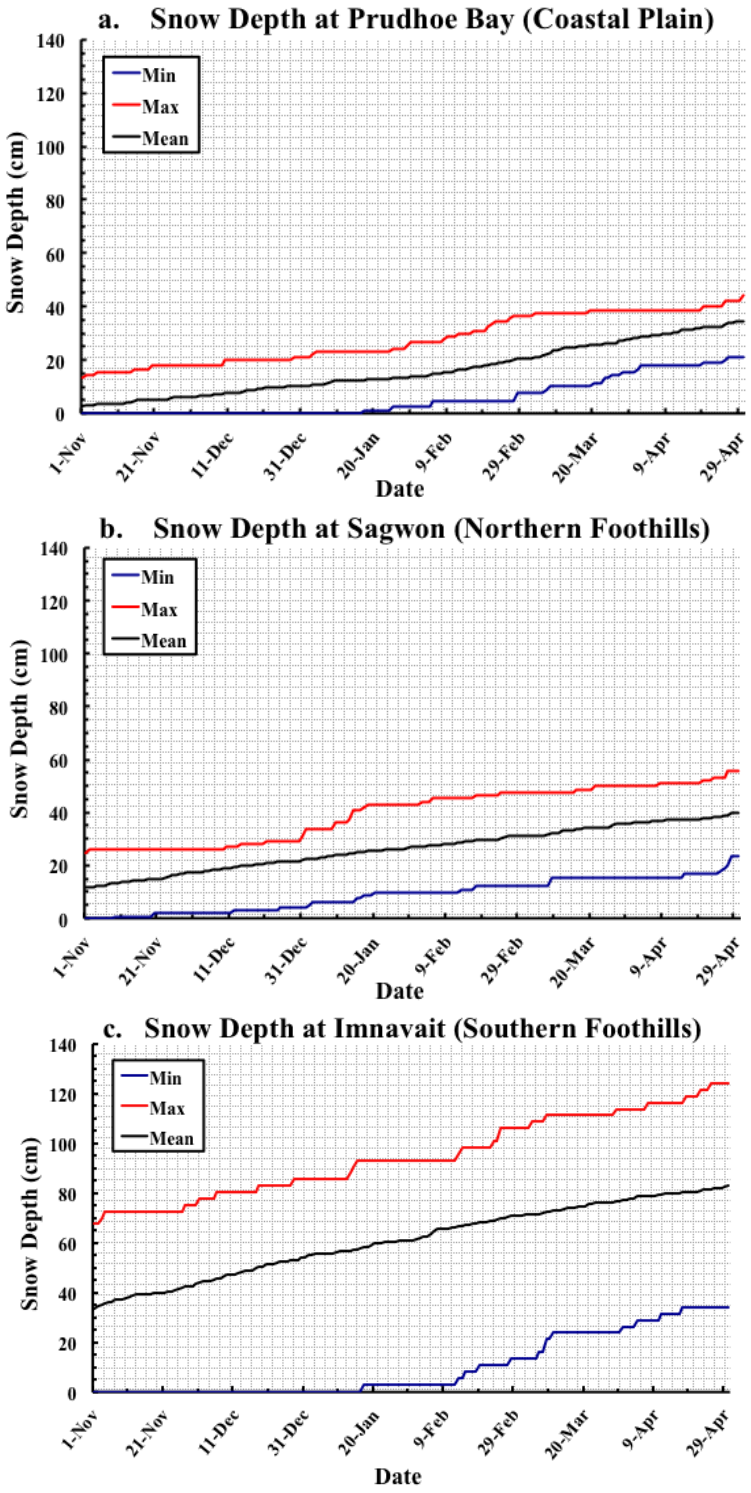

Figure V-16 displays maximum snow depths at Prudhoe Bay, Sagwon, and Imnavait estimated and observed between 2005 and 2013. Only the years 2005 to 2013 are shown because precipitation data did not become available at Prudhoe Bay until 2005 and thus, snow depths could only be estimated from 2005 and onward. All sites show substantial increases in snow depth. Prudhoe Bay had the lowest snow accumulation of the sites with a mean of 34.5 cm. Maximum snow depth at Prudhoe Bay increased by 1.0 cm per year over the period estimated and observed.

Sagwon showed the greatest estimated increase in snow depth at 4.0 cm per year, while estimated maximum snow depth at Imnavait increased by 2.7 cm per year. The mean maximum snow depth was 39.3 cm at Sagwon, and 78.4 cm at Imnavait. Overall, estimated snow depth showed an increasing trend at all SNOTEL sites, with Imnavait exhibiting the greatest maximum snow depths and precipitation.

Figure V-16 Maximum snow depth estimated and observed at SNOTEL sites between 2005 and 2013.

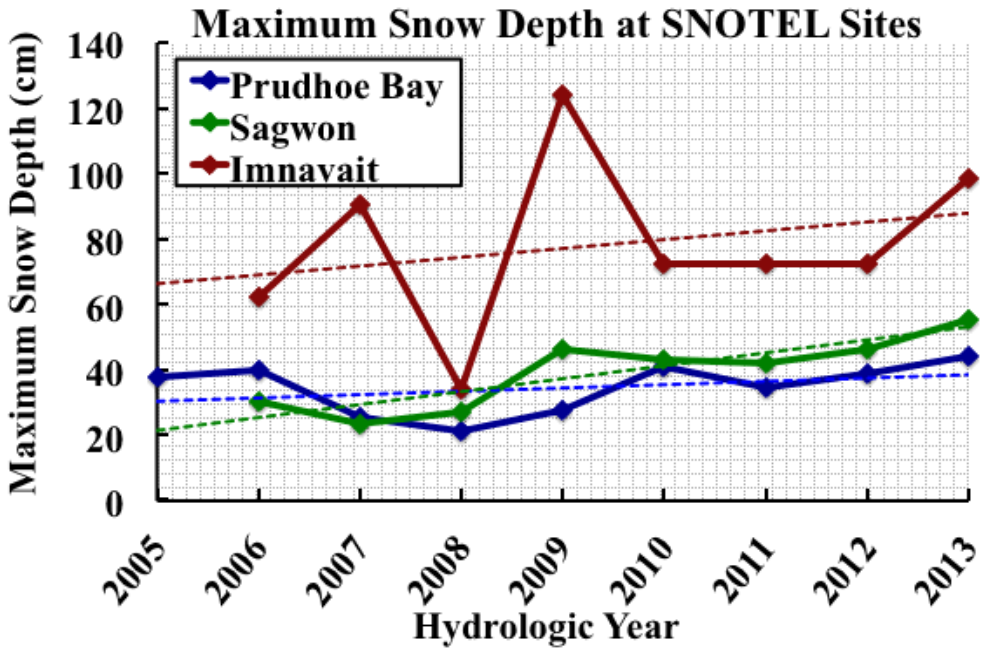

The three graphs in Figure V-17 show a comparison between the changes in estimated snow depth and the daily precipitation at Prudhoe Bay (a), Sagwon (b), and Imnavait (c). These graphs reveal that precipitation and snow depth do not change at similar times or amounts. Daily snow-depth data were available each day and thus, both positive and negative values are shown to illustrate changes in snow depth. The greater daily changes in snow depth compared to daily changes in precipitation reveals that snow depth cannot be determined using exclusively precipitation.

Figure V-17 Change in estimated snow depth versus precipitation at Prudhoe Bay (a), Sagwon (b), and Imnavait (c), using SNOTEL data.

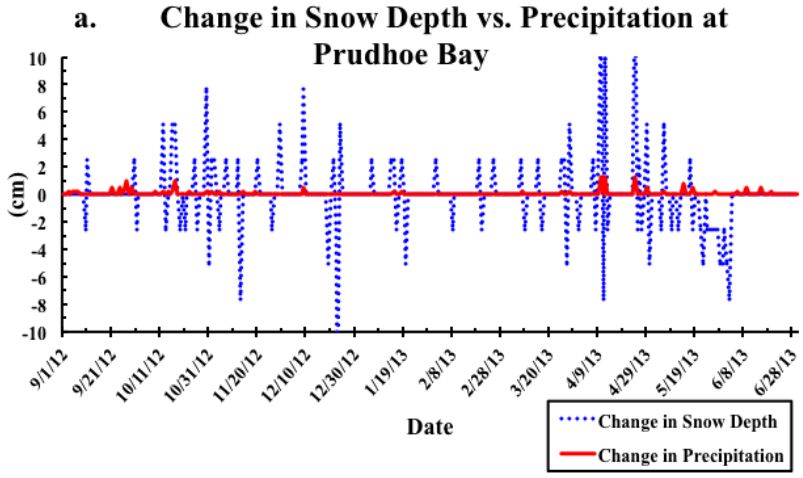

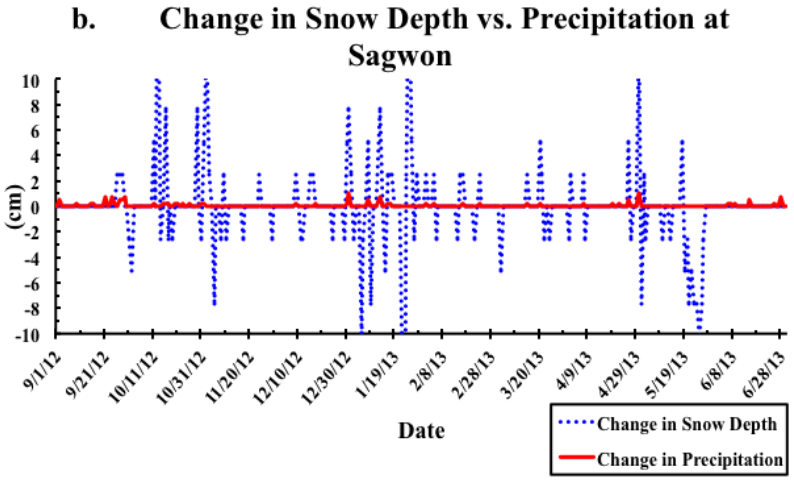

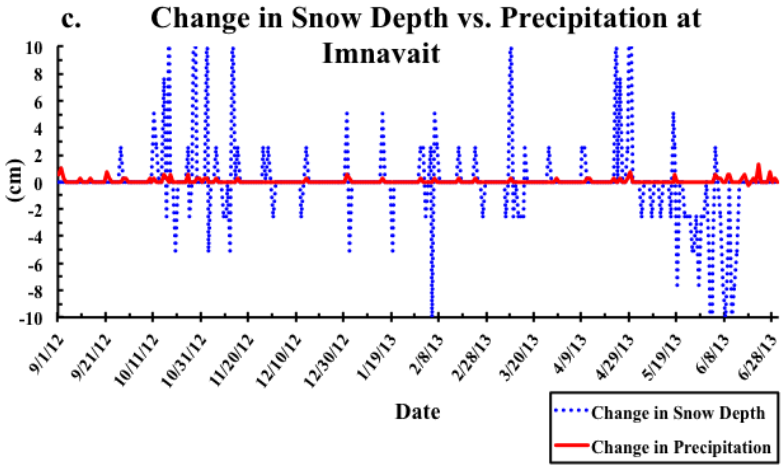

V.5 Conclusion

Overall, snow-cover characteristics exhibit substantial spatial variability within and between CALM sites. Results showed that air and soil-surface temperature dataloggers produced opposite trends for SCD in the two subzones. The shortening SCD in subzone D was mostly attributable to later dates of snow onset rather than earlier dates of snowmelt, while the lengthening trend in SCD in subzone E is attributable to both earlier dates of snow onset and later dates of snowmelt. This study tried to be consistent in applying the methodology to estimate SCD using the temperature dataloggers but in 1996 the soil-surface temperature amplitude observations frequently became greater than 1°C during the early winter at most sites in subzone E, and this is why SCD was shorter that year. Snow cover can be very thin in the Arctic because of wind and low precipitation totals and thus perhaps an extremely thin snow cover occurred during the 1996 hydrologic year, which limited the buffering effect of snow on the ground.

Snow depth estimates made using the iButton vertical arrays proved to be very difficult and time consuming, making the iButtons analysis done here less successful than in previous studies. The time-lapse cameras were found to be a more effective technique for making snow-depth observations. However, snow-depth observations made from January to March were not always decipherable because of darkness and harsh weather. Snow depth was found to be different between CALM sites and nearby SNOTEL sites, and this was likely attributable to the local topographic differences between the sites. Snow depth is known to be dependent upon other factors besides precipitation. The extrapolation of snow depth at SNOTEL sites revealed greater snow depths at the higher southern sites in the Arctic foothills as would be expected. These findings are consistent

with earlier findings in Chapter IV, which found winter soil-surface temperatures to be generally warmer at southern CALM sites in subzone E.

VI. Relations Between Soil-Surface Temperatures and Snow-Cover Characteristics

VI.1 Introduction

This chapter seeks to describe the relation between soil-surface temperature and snow-cover characteristics. The high degree of variability in soil-surface temperatures over short distances in the Kuparuk region is attributable to regional and local differences in land cover such as local vegetation, snow cover, microtopography, and soil conditions (Klene et al., 2001b; Klene et al., 2008). Previous studies in the region have found snow to be the main determinant of soil temperatures in the winter and soil-surface temperatures are found to increase as snow depth increases (Hinkel et al., 2008). This project utilizes the winter n-factor, which is the ratio of seasonal freezing degree-day sums at the soil-surface (FDD_s) to freezing degree-days in the air (FDD_a) (Carlson, 1952). Variability of winter n-factors at CALM sites is compared to both soil-surface and air temperature data, as well as snow-pack characteristics discussed in the previous Chapter V.

VI.2 Background

Previous studies have evaluated the spatial variability of n-factors at different scales and in a variety of settings including regional studies of the Kuparuk region (Klene et al., 2001b), local studies within 1-ha plots (Klene et al., 2008), and urban and rural settings (Hinkel et al., 2008). Winter n-factors with a value below 1 indicate colder air temperatures than those at the soil-surface. A study by Klene et al. (2008) in the Kuparuk

region found winter n-factors to be larger at northern sites (0.51 to 0.58), than southern sites (0.32 to 0.28). This spatial variability of n-factors was attributed to the microtopography and vegetation differences between the study sites (Klene et al., 2008). Another study evaluated the variability of winter n-factors in both urban and rural settings in Barrow, Alaska, located in subzone C (Hinkel et al., 2008). Winter n-factors were found to be higher in rural areas near the coast, and lower in urban areas where there was reduced snowdrift. The study found snow to be the greatest determinant of variability in winter n-factors within the study area (Hinkel et al., 2008).

N-factors have previously been used in the Stefan solution, which is a formula used to predict ALT (Lunardini, 1981). Variables used in the equation include air temperature, soil density, and moisture, among others, and some estimations have utilized summer and/or winter n-factors. In the Kuparuk River study area, when air temperature measurements and three-year mean summer n-factors were used in a spatial implementation of the equation, the results were an average of 18 % different from measured values of ALT (Klene et al., 2011b). When measured air temperatures were used without summer n-factors in the equation, the estimated ALT had a 29 % mean difference from observed. Thus, the utilization of the n-factor in the Stefan solution was found to be effective in predicting ALT in the Kuparuk (Klene et al., 2001b).

VI.3 Methodology

VI.3.1 Data Availability

CALM air and soil-surface temperature data were used to calculate winter n-factors at each CALM site. Air temperature data from an additional observation site (Happy Valley) was also utilized. CALM temperature data collection was described in Chapter IV and CALM study site locations and additional sites are shown in Figure IV-1. Snow depth estimates and observations described in Chapter V (using SNOTEL snow depth and precipitation data) are related to winter n-factors in this chapter.

VI.3.2 Data Analysis

Winter n-factors were calculated at each CALM site for each winter season, which was defined as November 1 to April 31 each year. The winter season did not start until November because positive values of snow depth were not estimated with the regression equations at all sites until then. The following equation was used to calculate the winter n-factor:

Equation VI-1.

$$n = FDD_s / FDD_a$$

where n is the winter n-factor, FDD_s is the sum of the absolute value of all soil-surface temperatures less than 0 °C, and FDD_a is the sum of the absolute value of all air temperatures less than 0 °C during the winter season.

Only years with a complete set of air and soil-surface temperature data during the winter season could have an n-factor calculated. Days with missing air temperature data were interpolated using a linear-regression analysis, based upon a relationship between air temperatures at CALM sites with missing data, and air temperatures from one nearby CALM site or supplemental observation site. For the missing air temperatures at sites U7c (hydrologic years 1999 and 2000), U11c (2007, 2009, 2011) and U10 (2009, 2011, 2012), linear regressions between CALM sites U7b, U11b, and an additional site (Happy Valley), respectively, were done. The locations of CALM sites and supplemental observation sites are shown in Figure IV-1. The mean monthly (November to April) and mean annual winter n-factors for all years between 1996 and 2013 were determined for each site. Both mean monthly and mean winter n-factors were also aggregated into subzones (subzone D = U7b, U7c, and U31; subzone E = U32a, U32b, U10, U11b, U11c, and U12) by averaging the mean winter n-factors between all sites in the subzone.

VI.4 Results

The mean FDD_a show a distinct north to south progression in Figure VI-1, with winter temperatures typically being colder at northern CALM sites in subzone D (U7b, U7c, and U31). Site U31 experienced the coldest winter air temperatures and had the highest maximum, mean, and minimum FDD_a. Sites located in subzone E experienced the warmest winter air temperatures.

Figure VI-1 Box-and-whisker plot showing the median, quartiles, and range of FDD_a at each of the 9 CALM sites observed between 1996 and 2013. Sites are shown in a north-south transect (left to right).

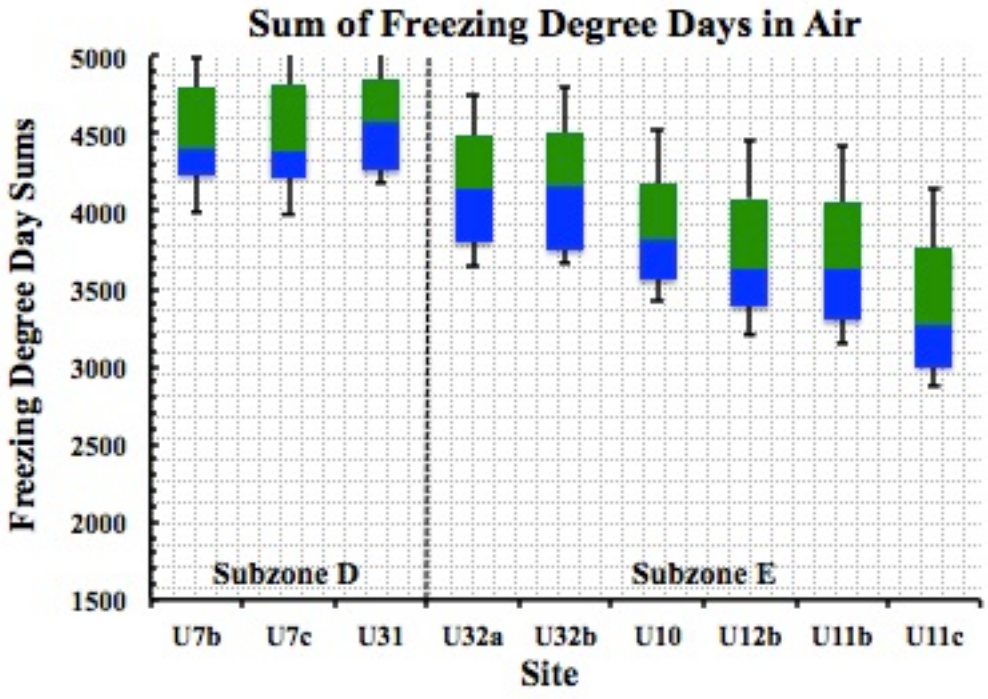

The variability of FDD_s at CALM sites is displayed in Figure VI-2. Northern sites U7b and U7c were found to have the greatest FDD_s, and this is likely attributable to the snow pack on the coastal plain. Site U31 is located at the most continental extent of the coastal plain and had the lowest mean FDD_s. The low FDD_s at site U31 may be

attributable to the greater snow depths observed there (Chapter V). Sites U32a, U32b, and U10 are located in the northern Arctic foothills where the topography and taller vegetation limit wind redistribution and allow for a thicker snowpack. Soil-surface temperatures were generally warmer at these sites than those on the coastal plain. Finally, the lowest FDD_s were observed at sites U12b, U11b, and 11c, in the southern Arctic foothills. This again, is partly attributable to the topography and taller vegetation, which are greatest at these CALM sites.

Figure VI-2 Box-and-whisker plot showing the median, quartiles, and range of FDD_s at each CALM site observed between 1996 and 2013. Sites are shown in a north to south progression (left to right).

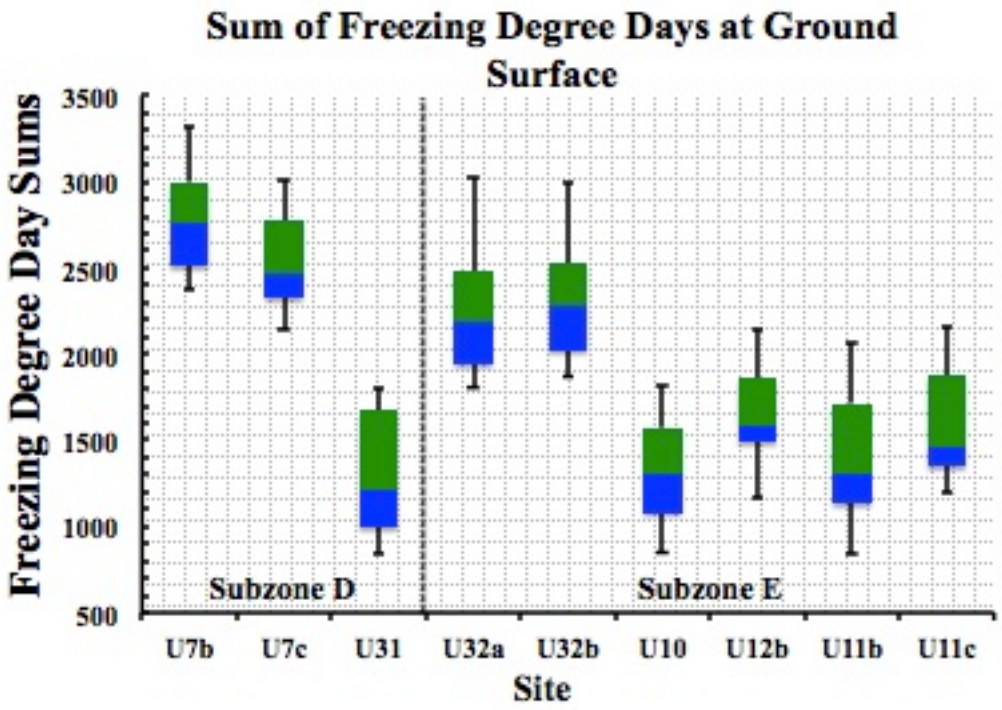

Summary statistics for winter n-factors observed at CALM sites between 1996 and 2013 are shown in Table VI-1. The highest winter n-factors occurred at sites closer to the coast in the north. The high winter n-factors observed further north reflect the thin snow cover and short tundra vegetation that characterize the arctic coastal plain and allow greater heat loss through the snowpack. Sites located further south experienced winter n-factors with a slightly greater variation around the mean.

Table VI-1 Winter n-factor minimum, mean, median, maximum, range and standard deviation observed between 1996 and 2013 at each site, which are listed from north to south in columns left to right.

	Subzone D			*Subzone E*					
	U7b	**U7c**	**U31**	**U32a**	**U32b**	**U12b**	**U11b**	**U11c**	**U10**
Minimum	0.48	0.43	0.17	0.36	0.44	0.24	0.15	0.27	0.17
Mean	0.60	0.55	0.24	0.52	0.55	0.40	0.33	0.44	0.30
Median	0.60	0.57	0.23	0.51	0.55	0.43	0.31	0.46	0.30
Maximum	0.71	0.65	0.39	0.63	0.69	0.55	0.50	0.61	0.45
Range	0.24	0.22	0.23	0.28	0.25	0.31	0.34	0.34	0.29
Std. Dev.	0.05	0.07	0.07	0.07	0.07	0.08	0.11	0.09	0.09

Winter n-factors at each CALM site during the study period are shown in Figure VI-3. Site U31 exhibited the lowest n-factor during most years, largely due to it typically having the greatest FDD_a sum and lowest sum of FDD_s of all the sites. Besides site U31, the graph indicates that northern sites (U7b and U7c) had higher winter n-factors than southern sites (U11b, U11c, and U10), which had the lowest.

Figure VI-3 A time-series of winter n-factors at CALM sites between 1996 and 2013.

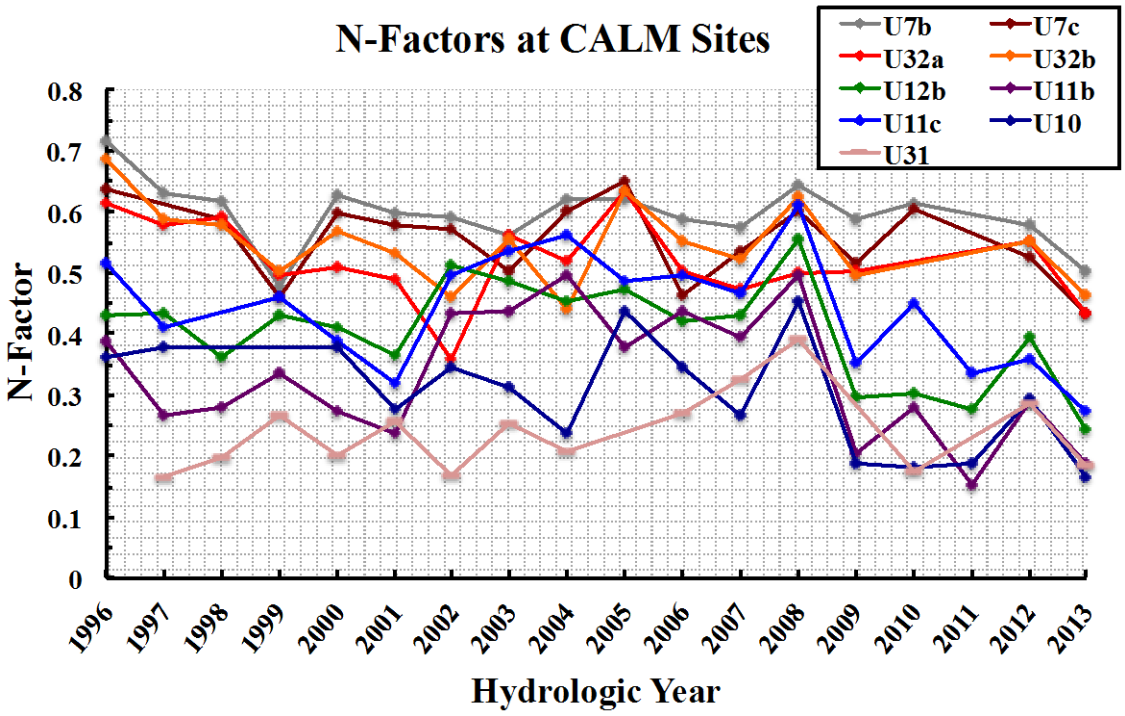

Table VI-2 displays summary statistics for mean winter n-factors observed in subzones D and E between 1996 and 2013. These statistics were derived from the mean winter n-factor recorded at each CALM site over the study period. Subzone D recorded greater minimum, mean, median, and maximum winter n-factors than subzone E. The range and standard deviation of winter n-factors was smaller in subzone D than E, reflecting less variation between sites and less interannual variability in subzone D.

Table VI-2 Summary statistics of winter n-factors observed in subzones D and E between 1996 and 2013.

	Subzone D	Subzone E
Minimum	0.36	0.27
Mean	0.46	0.42
Median	0.47	0.43
Maximum	0.59	0.57
Range	0.23	0.30
Std. Dev.	0.06	0.09

The mean winter n-factors remained relatively stable in subzone D and decreased in subzone E by a magnitude of 0.008 each year, Figure VI-4. Years for which calculated winter n-factor were not available for all sites in the subzone are represented as single points on the graph and were not used to calculate the trend. For instance, only two sites (U7b and U7c) had sufficient data to calculate winter n-factors in 2005 and thus the mean winter n-factor from these sites (0.65) is represented as a single point. The mean winter n-factor for the entire study period was 0.46 in subzone D and 0.42 in subzone E. The slightly higher n-factors found in subzone D may be attributable to its location on the Arctic coastal plain, which has thinner snow cover. Both subzones had a value of 0.54 for the winter n-factor in 2008. The lowest mean winter n-factor in both subzones occurred in 2013.

Figure VI-4 Time-series of mean winter n-factors for subzones D and E between 1996 and 2013. Point data values represent years when not all sites in the subzone had sufficient data to calculate n-factors.

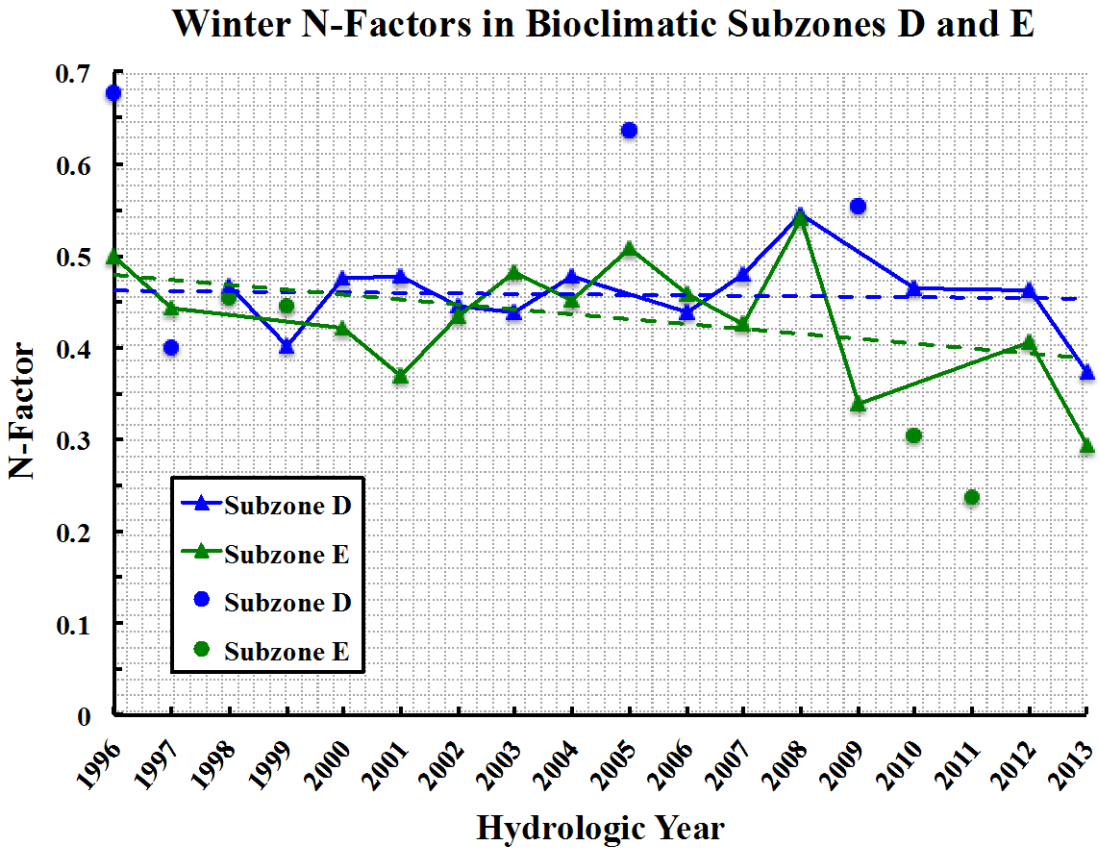

Mean annual winter n-factors in both subzones are negatively correlated with estimated maximum snow depth calculated from SNOTEL precipitation data (Figure VI-5). Only years that had snow-depth estimates for all sites in the subzone were included. Overall, winter n-factors decrease at very similar rates in each subzone as snow depth increases. The winter n-factors in subzones D and E decreased by a magnitude of 0.005 and 0.004, respectively, for each centimeter increase in snow depth.

Figure VI-5 Correlation between mean annual winter n-factors and estimated maximum snow depths for subzones D and E from 2005 to 2013.

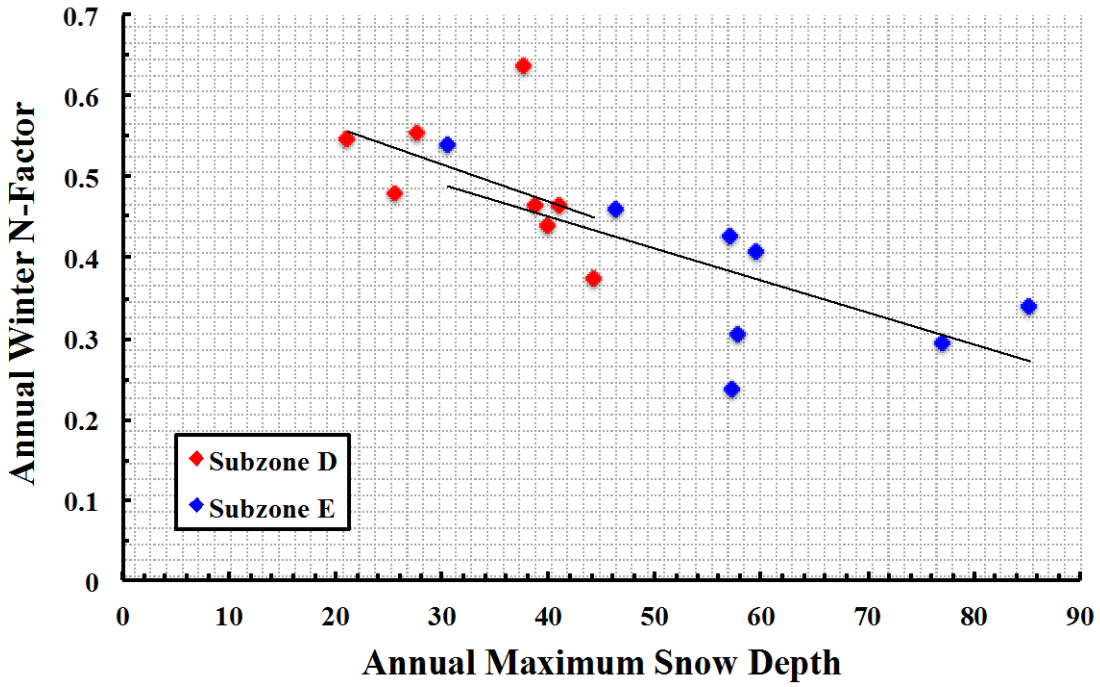

The distribution of winter n-factors at each CALM site between 1996 and 2013 are displayed in Figure VI-6. Sites U7b and U7c had the greatest n-factors, which may be attributable to the greater FDD_s experienced at those sites. The lowest winter n-factors were observed at site U31, which had the greatest FDD_a and the lowest FDD_s. Except for site U31, winter n-factors show a generally declining trend to the south and higher elevations. Southern sites had the lowest n-factors and the greatest range between minimum and maximum winter n-factors. The greater range in values at southern sites may be attributable to the larger variability in vegetation and microtopography in subzone E.

Figure VI-6 Box and whisker plot showing the median, quartiles, and range of winter n-factors at each CALM site observed between 1996 and 2013. Sites are listed in a north to south progression (left to right).

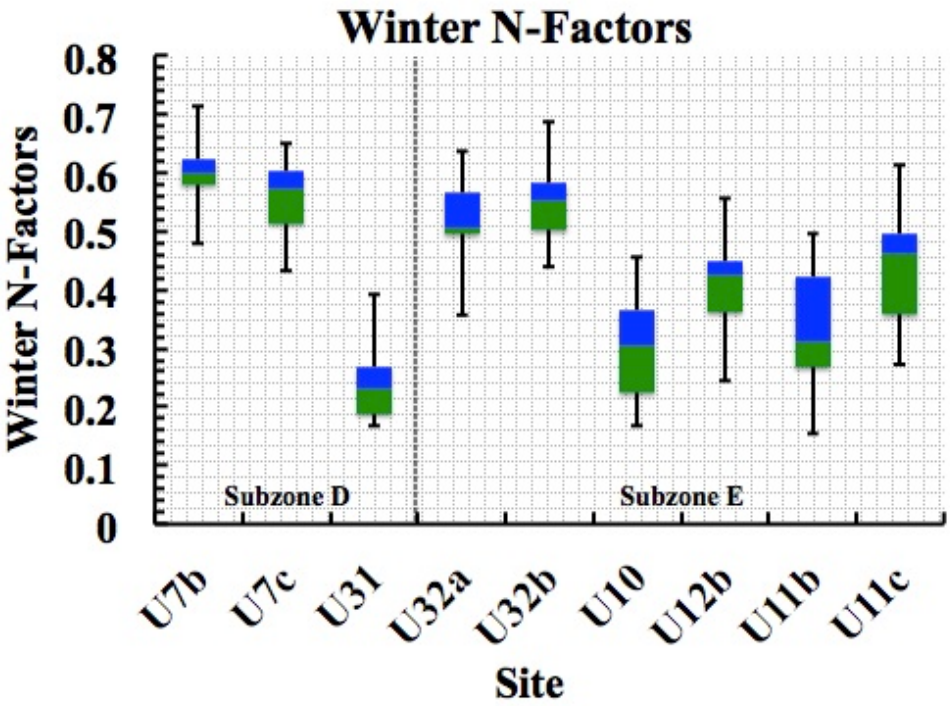

Figure VI-7 shows no relationship between winter n-factors and FDD_a. The lowest winter n-factor (0.15) was measured at site U11b in 2011, while the greatest winter n-factor (0.71) was measured at site U7b in 1996. Sites U7b, U7c, and U31 are all located on the coastal plain and have similar FDD_a. However, site U31 had significantly lower n-factors than those observed at sites U7b and U7c, indicating that the FDD_a is not the main determinant of winter n-factors.

Figure VI-7 Relation between FDD_a and winter n-factors between 1996 and 2013 at CALM sites.

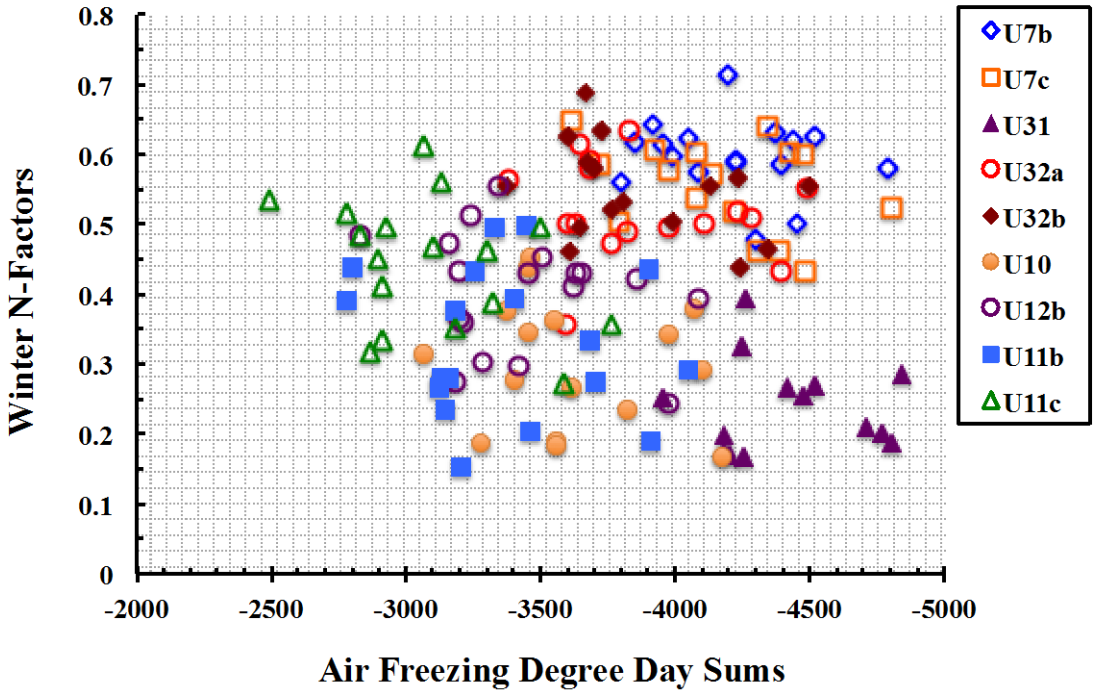

The relationship between winter n-factors and FDD_s exhibits a clear trend, which indicates a direct relationship exists between the two parameters (Figure VI-8). As the FDD_s increases, the winter n-factor also increases. The low FDD_s at site U31 caused it to have significantly lower winter n-factors than sites U7b and U7c, reflecting the warmer soil temperatures in spite of the cold air temperatures. Thus, the lower FDD_s at site U31 also reflect the greater snow depths.

Figure VI-8 Relation between FDD_s and winter n-factors at CALM sites between 1996 and 2013.

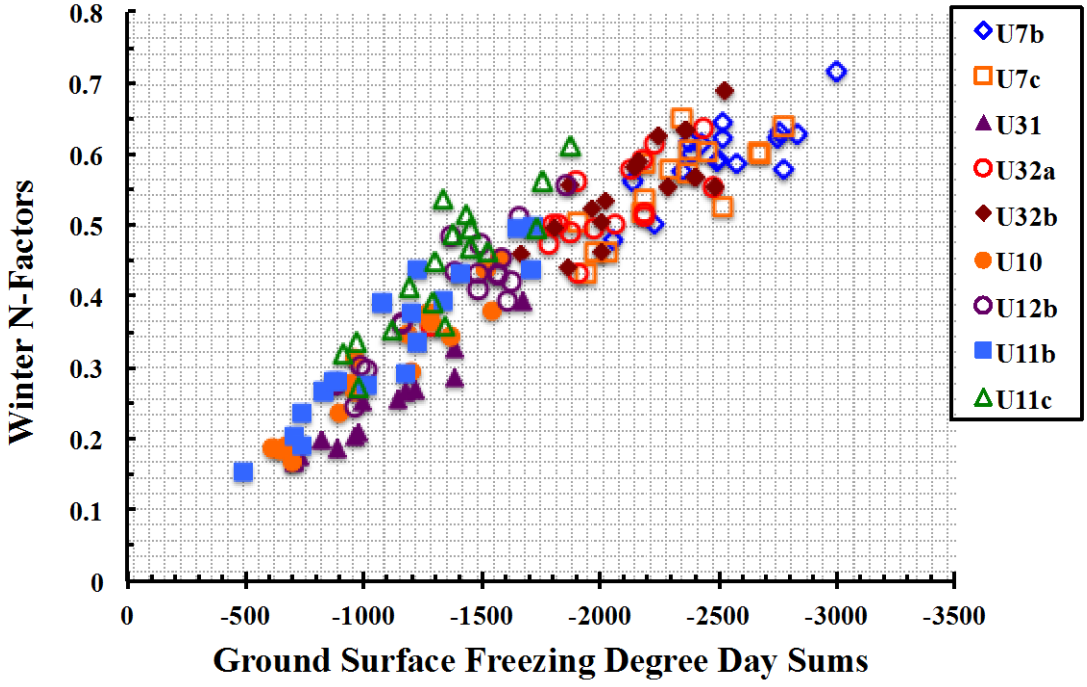

VI.5 Conclusions

The relationship between snow-cover characteristics and soil-surface temperatures is apparent when the winter n-factor is utilized. Similar to previous studies, this chapter found the winter n-factor to be strongly dependent upon soil-surface temperatures and thus snow-cover characteristics.

These conclusions are illustrated by results from site U31. Site U31 had the lowest FDD_s and lowest winter n-factors. Snow-depth measurements at site U31 made using time-lapse cameras (Chapter V) indicate that it had a greater snow depth than nearby site U32b or site U11b to the south. Soil-surface temperatures are known to be strongly influenced by snow cover and since site U31 had the greatest snow depth, the low winter n-factors may be attributable to that. All other CALM sites show a north to south progression of decreasing mean winter n-factors, and previous snow depth estimates (Chapter V) show an increase in snow accumulation from north to south in the region, which also reflects the general elevational trend. Overall, the spatial variability of winter soil-surface temperatures is strongly dependent on snow cover characteristics.

VII. Conclusions

VII.1 Summary of Results

Soil-surface temperatures exhibit substantial spatial variability during the winter between point locations in the study area. This study explored the relationship between soil-surface temperatures and snow cover in the Kuparuk River region of the North Slope of Alaska. To accomplish this, cameras and ground-based temperature observations collected at CALM sites in different microtopographic settings were used to describe snow-cover characteristics. Unfortunately, several of these techniques had either high failure rates or produced short observational records because of environmental and logistical limitations, which resulted in inconsistent snow data. To supplement snow-depth measurements made in this study using vertical arrays of temperature dataloggers and time-lapse cameras, measurements were compared to snow depth data collected by nearby USDA SNOTEL sites. Snow cover exhibited substantial spatial variability between nearby sites (CALM and SNOTEL sites) and overall, snow depths were found to generally be different in the coastal plain and foothills physiographic provinces, and bioclimatic subzones.

The relationship between the spatial variability of snow and soil-surface temperatures was examined using winter n-factors. Winter n-factors have a direct relationship with soil-surface temperatures, making them strongly dependent on snow-cover conditions. Larger winter n-factors were measured in areas with lower winter soil-surface temperatures, and it was in these areas that thinner snow covers were observed in this study. Overall, snow tends to insulate the underlying ground and the large spatial

variability in winter soil-surface temperatures was strongly dependent upon snow depth. Understanding snow cover characteristics at point locations in the Arctic can be used to infer the state of the winter ground thermal regime, which provides insight into possible ecological disturbances.

VII.2 Suggestions for Future Research

To improve upon this research, changes in the methods tested to measure snow cover in Chapter V should be considered. Snow-cover duration estimates made using air and soil-surface temperature dataloggers produced results in most years however these were likely underestimated. Images from time-lapse cameras revealed snow on the ground longer than indicated by the dataloggers, particularly during the snowmelt period. For instance, time-lapse cameras estimated the date of snowmelt at site U32b to be 8 June while the methodology using temperature dataloggers estimated it to be 21 May. SCD was underestimated because the methodology developed in Chapter V required air temperatures to remain below 0 °C in the spring. Therefore, a new technique that utilizes both cameras and soil-surface temperature data is suggested. The cameras were often unsuccessful at taking images during the winter months yet were more reliable during the spring snowmelt. More reliable measurements would allow the relationship between soil-surface temperature variability and snow-cover characteristics to be better analyzed and thus, provide a better insight into the winter ground thermal regime and possible ecosystem changes associated with warming soils.

VIII. References

Adams, E. E., Slaughter, A. E., McKittrick, L., & Miller, D. A. (2011). Local Terrain-topography and Thermal-properties Influence on Energy and Mass Balance of a Snow Cover. Annals of Glaciology, 52(58), 169-175.

Bonfils, C. J. W., Phillips, T. J., Lawrence, D. M., Cameron-Smith, P., Riley, W. J., & Subin, Z. M. (2012). On the Influence of Shrub Height and Expansion on Northern High Latitude Climate. Environmental Research Letters, 7(1). doi: 10.1088/1748-9326/7/1/015503

Burn, C. R., & Smith, C. A. S. (1988). Observations of the "Thermal Offset" in Near-Surface Mean Annual Ground Temperatures at Several Sites near Mayo, Yukon Territory, Canada ARCTIC, 41(2), 99-104.

Callaghan, T. V., Johansson, M., & Brown, R. D. (2011a). The Changing Face of Arctic Snow Cover: A Synthesis of Observed and Projected Changes Royal Swedish Academy of Sciences, 40(1), 17-31. doi: 10.1007/s13280-011-0212-y

Callaghan, T. V., Johnasson, M., Brown, R. D., Groisman, P. Y., Labba, N., Radionov, V., Bradley, R. S., Blangy, S., Bulygina, O. N., Christensen, T. R., Colman, J. E., Essery, R. L. H., Forbes, B. C., Forchhammer, M. C., Goludev, V. N., Honrath, R. E., Juday, G. P., Meshcherskaya, A. V., Phoenix, G. K., Pomeroy, J., Rautio, A., Robinson, D. A., Schmidt, N. M., Serreze, M. C., Shevchenko, V. P., Shiklomanov, A. I., Shmakin, A. B., Skold, P., Sturm, M., Woo, M. & Wood, E. F. (2011b). Multiple Effects of Changes in Arctic Snow Cover Royal Swedish Academy of Sciences, 40(1), 32-45. doi: 10.1007/s13280-011-0213-x

Calonne, N., Flin, F., Lesaffre, S., Roscoat, R. D., & Geindreau, C. (2011). Numerical and Experimental Investigations of the Effective Thermal Conductivity of Snow. Geophysical Research Letters, 38(23). doi: 10.1029/2011GL049234

Carlson, H. (1952). Calculation of Depth of Thaw in Frozen Ground. *Highway Research Board Special Report*(2), 192- 223.

Clilverd, H. M., White, D. M., Tidwell, A. C., & Rawlins, M. A. (2011). The Sensitivity of Northern Groundwater Recharge to Climate Change: A Case Study in Northwest Alaska. Journal of the American Water Resources Association, 47(6), 1228-1240.

Decker, K. L. M., Wang, D., Waite, C., & Scherbatskoy, T. (2003). Snow Removal and Ambient Air Temperature Effects of Forest Soil Temperatures in Northern Vermont Soil Science Society of America, 67(4), 1234-1242.

Dozier, J., & Painter, T. H. (2004). Multispectral And Hyperspectral Remote Sensing Of Alpine Snow Properties. Annual Review of Earth and Planetary Sciences, 32, 465-494. doi: 10.1146/annurev.earth.32.101802.120404

French, H. M. (2007). The Periglacial Environment (3 ed.). The Atrium, Southern Gate, Chichester, West Sussex P019 8SQ, England: John Wiley & Sons.

Gouttevin, I., Menegoz, M., Domine, F., Krinner, G., Koven, C., Ciais, P., Tarnocai, C. & Boike, J. (2012). How the Insulating Properties of Snow Affect Soil Carbon Distribution in the Continental Pan-Arctic Area. Journal of Geophysical Research: Biogeosciences, 117(G02020). doi: 10.1029/2011JG001916

Hall, D. K., Chang, A. C., & Foster, J. L. (1986). Detection of the Depth-hoar Layer in the Snow-pack of the Arctic Coastal Plain of Alaska, U.S.A., Using Satellite Data. Journal of Glaciology 32(110), 87-94.

Hall, D. K., Riggs, G. A., Salomonson, V. V., DiGirolamo, N. E., & Bayr, K. J. (2002). MODIS snow-cover products. Remote Sensing of the Environment, 83, 181-194.

Hartmann, D. D., Tank, A. M. G. K., Rusticucci, M., Alexander, L. V., Bronnimann, S., Charabi, Y., Dentener, F. J., Dlugokencky, E. J., Easterling, D. R., Kaplan, A., Soden, B. J., Thorne, P. W., Wild, M. & Zhai, P. M. (2013). 2013: Observations: Atmosphere and Surface. In T. F. Stocker, D. Qin, G.-K. Plattner, M. Tignor, S.K. Allen, J. Boschung, A. Nauels, Y. Xia, V. Bex and P.M. Midgley (Ed.), Climate Change 2013: The Physical Science Basis. Contribution of Working Group I to the Fifth Assessment Report of the Intergovernmental Panel on Climate Change (pp. 159-254). Cambridge, United Kingdom and New York, NY, USA: Cambridge University Press.

Hinkel, K. M., Klene, A. E., & Nelson, F. E. (2008). Spatial and interannual patterns of winter N-factors near Barrow, Alaska. Paper presented at the Ninth International Conference on Permafrost, Institute of Northern Engineering: University of Alaska Fairbanks.

Holmgren, J., Sturm, M., Yankielun, N. E., & Koh, G. (1998). Extensive Measurements of Snow Depth Using FM-CW Radar. Cold Regions Science and Technology, 27(1), 17-30.

Klene, A. E., Nelson, F. E., & Shiklomanov, N. I. (2001a). The N-Factor as a Tool in Geocryological Mapping: Seasonal Thaw in the Kuparuk River Basin, Alaska. Physical Geography, 22(6), 449-466. doi: 10.1080/02723646.2001.10642754

Klene, A. E., Nelson, F. E., Shiklomanov, N. I., & Hinkel, K. M. (2001b). The N-factor in Natural Landscapes: Variability of Air and Soil-Surface Temperatures Kuparuk River Basin, Alaska, U.S.A. Arctic, Antarctic, and Alpine Research, 33(2), 140-148. doi: 10.2307/1552214

Klene, A. E., Nelson, F. E., Shiklomanov, N. I., & Streletskiy, D. A. (2008). Interannual Variability of Winter N-Factors in the Kuparuk River Basin, Alaska. Paper presented at the Proceedings of the Ninth International Conference on Permafrost.

Laffley, D., Bernard, E., Griselin, M., Tolle, F., Friedt, J.-M., Martin, G., & Marlin, C. (2012). High Temporal Resolution Monitoring of Snow Cover Using Oblique View Ground-based Pictures. Polar Record 48(01), 11-16. doi: 10.1017/S0032247411000519

Lewkowicz, A. G. (2008). Evaluation of Miniature Temperature-loggers to Monitor Snowpack Evolution at Mountain Permafrost Sites, Northwestern Canada. Permafrost and Periglacial Processes, 19(3), 323-331. doi: 10.1002/ppp.625

Liston, G. E., & Sturm, M. (2002). Winter Precipitation Patterns in Arctic Alaska Determined from a Blowing-Snow Model and Snow-Depth Observations. Journal of Hydrometeorology, 3(6), 646-659.

Lunardini, V. J. (1981). *Heat Transfer in Cold Climates*. New York: Van Nostrand Reinhold.

Maxwell, B. (1992). Arctic Ecosystems in a Changing Climate: An Ecophysiological Perspective. F. S. Chapin III, R. I. Jefferies, J. F. Reynolds, G. R. Shaver &J. Svoboda (Ed.), (pp. 11-34). San Diego: Academic Press, Inc.

McBean, G. (2005). Arctic Climate: Past and Present. Carolyn Symon, Lelani Arris & Bill Heal (Ed.), Arctic Climate Impact Assessment (pp. 21-60). New York, NY: Cambridge University Press.

Morse, P. D., Burn, C. R., & Kokeli, S. V. (2012). Influence of Snow and Near-surface Ground Temperatures in Upland and Alluvial Environments of the Outer Mackenzie Delta. Canadian Journal of Earth Sciences, 49(8), 895-913. doi: 10.1139/e2012-012

Natural Resources Conservation Service. National Water & Climate Center. http://www.wcc.nrcs.usda.gov/snotel/Alaska/alaska.html

Nyland, K. E., Shiklomanov, N. I., Streletskiy, D. A., Klene, A. E., & Nelson, F. E. (2012). Effect of Vegetation on Soil-Surface Temperatures in Northern Alaska. Paper presented at the 10th International Conference on Permafrost, Salekhard, Russia.

Oke, T. R. (1978). Boundary Layer Climates. London: Methuen.

Olsen, T. V., Callaghan, J. D. R., Reiersen, L. O., Dahl-Jensen, D., Granskog, M. A., Goodison, G. K. H., Johansson, M., Kallenborn, R., Key, J., Klepikov, A., Meier, W., Overland, J. E., Prowse, T. S., Sharp, M., Vincent, W. F. & Walsh, J. (2011). The Changing Arctic Cryosphere and Likely Consequences: An Overview. AMBIO, 40 111-118. doi: 10.1007/s13280-011-0220-y

Sazonova, T. S., & Romanovsky, V. E. (2003). A Model for Regional-scale Estimation of Temporal and Spatial Variability of Active Layer Thickness and Mean Annual Ground Temperatures. Permafrost and Periglacial Processes, 14(2), 125-139. doi: 10.1002/ppp.449

Schmidt, G., & Wolfe, J. (2009). Climate Change: Picturing the Science. New York: WW Norton.

Shiklomanov, N. I., Streletskiy, D. A., & E., N. F. (2012). Northern Hemisphere Component of the Global Circumpolar Active Layer Monitoring (CALM) Program. Paper presented at the Proceedings of the 10th International Conference on Permafrost, Salekhard, Russia.

Shiklomanov, N. I., & Nelson, F. E. (2003). Climatic Variability in the Kuparuk Region, North-Central Alaska: Optimizing Spatial and Temporal Interpolation in a Sparse Observation Network. Arctic, 56(2), 136-146.

Shiklomanov, N. I., & Nelson, F. E. (2013). Treatise on Geomorphology: Elsevier Inc.

Shiklomanov, N. I., Streletskiy, D. A., Nelson, F. E., Hollister, R. D., Romanovsky, V. E., Tweedie, C. E., Bockheim, J. G. & Brown, J. (2010). Decadal Variations of Active-layer Thickness in Moisture-controlled Landscapes, Barrow, Alaska. Journal of Geophysical Research, 115(G00I04). doi: 10.1029/2009JG001248

Smith, S. L., Romanovsky, V. E., Lewkowicz, A. G., Burn, C. R., Allard, M., Clow, G. D., Yoshikawa, K. & Throop, J. (2010). Thermal State of Permafrost in North America: A Contribution to the International Polar Year. Permafrost and Periglacial Processes, 21, 117-135. doi: 10.1002/ppp.690

Stieglitz, M., Dery, S. J., Romanovsky, V. E., & Osterkamp, T. E. (2003). The Role of Snow Cover in the Warming of Arctic Permafrost. Geophysical Research Letters, 30(13). doi: 10.1029/2003GL017337

Streletskiy, D. A., Shiklomanov, N. I., Nelson, F. E., & Klene, A. E. (2008). Thirteen Years of Observations at Alaskan CALM Sites: Long-term Active Layer and Ground Surface Temperature Trends. Paper presented at the Ninth International Conference on Permafrost, Fairbanks, Alaska, Institute of Northern Engineering, University of Alaska Fairbanks.

Sturm, M., Holmgren, J., McFadden, J. P., Liston, G. E., Chapin, S. F., & Racine, C. H. (2001). Snow–Shrub Interactions in Arctic Tundra: A Hypothesis with Climatic Implications. Journal of Climate, 14(3), 336.

Sturm, M., Schimel, J., Michaelson, G., Welker, J. M., Oberbauer, S. F., Liston, G. E., Romanovsky, V. E. (2005). Winter Biological Processes Could Help Convert Arctic Tundra to Shrubland. BioScience, 55(1), 17-26. doi: 10.1641/0006-3568(2005)055[0017:WBPCHC]2.0.CO;2

Sturm, M., Taras, B., Liston, G. E., Derksen, C., Jonas, T., & Lea, J. (2010). Estimating Snow Water Equivalent Using Snow Depth Data and Climate Classes. Journal Hydrometeorology, 11(6), 1380-1394.

Throop, J., Lewkowicz, A. G., & Smith, S. L. (2011). Climate and ground temperature relations at sites across the continuous and discontinuous permafrost zones, Northern Canada. Canadian Journal of Earth Sciences, 49(8), 865-876. doi: 10.1139/e11-075

Wahrhaftig, C. (1965). Physiographic Divisions of Alaska (pp. 52). Washington: United States Government Printing Office.

Walker, D. A., Auerbach, N. A., Bockheim, J. G., Chapin, F. S., Eugster, W., King, J. Y., McFadden, J. P., Michaelson, G. J., Nelson, F. E., Oechel, W. C., Ping, C. L., Reeburg, W. S., Regli, S., Shiklomanov, N. I. & Vourlitis, G. L. (1998). Energy and trace-gas fluxes across a soil pH boundary in the Arctic. Nature, 394, 469-472. doi: 10.1038/28839

Walker, D. A., Raynolds, M. K., Daniels, F. J. A., Einarsson, E., Elvebakk, A., Gould, W. A., Katenin, A. E., Kholod, S. S., Markon, C. J., Meinikov, E. S., Moskalenko, N. G., Talbot, S. S. & Yurtsev, B. A. (2005). The Circumpolar Arctic Vegetation Map. Journal of Vegetation Science, 16, 267-282.

Wendler, G., Shulski, M., & Moore, B. (2010). Changes in the Climate of the Alaskan North Slope and the Ice Concentration of the Adjacent Beaufort Sea. Theoretical and Applied Climatology, 99(1-2), 67-74.

Zhang, Y., Wang, X., Fraser, R., Olthof, I., Chen, W., Mclennan, D., Ponomarenko, S. Wu, W. (2013). Modeling and Mapping Climate Change Impacts on Permafrost at High Spatial Resolution for an Arctic Region with Complex Terrain. The Cryosphere, 7, 1121-1137. doi: 10.5194/tc-7-1121-2013